Cell Reports

Resource

Representative Sequencing: Unbiased Sampling of Solid Tumor Tissue

Graphical Abstract

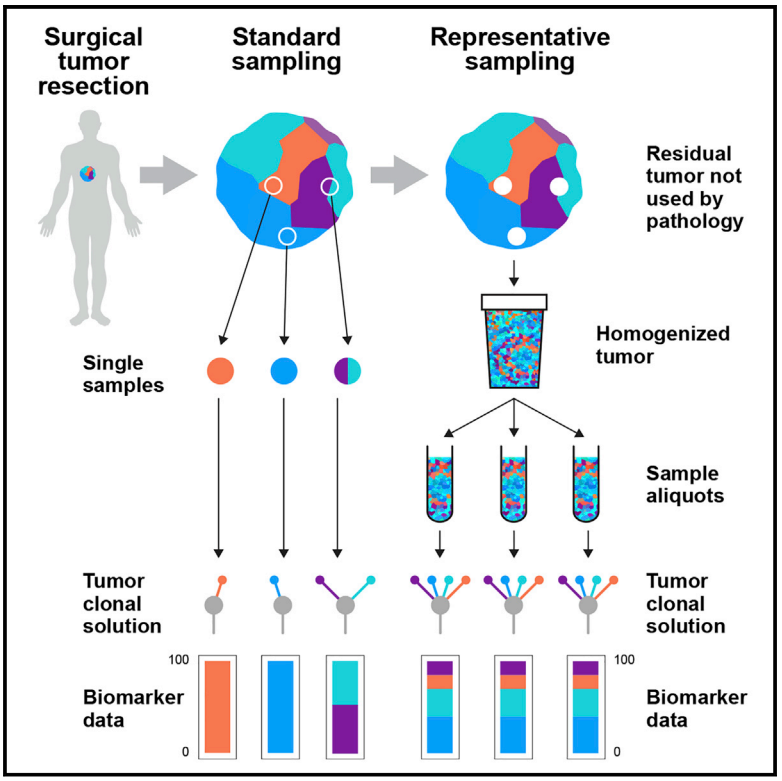

Highlights

- Representative sequencing (Rep-Seq) is a new method for tumor molecular profiling
- Rep-Seq homogenizes residual tumor tissue not taken for standard pathology
- Representative sampling of tumors generates accurate tumor mutation burden scores
- Rep-Seq detects more mutations and accurately resolves clonal from subclonal variants

Authors

Kevin Litchfield, Stacey Stanislaw, Lavinia Spain, ..., Charles Swanton, Nelson R. Alexander, Samra Turajlic

Correspondence

charles.swanton@crick.ac.uk (C.S.), nelson.alexander@roche.com (N.R.A.), samra.turajlic@crick.ac.uk (S.T.)

In Brief

Solid tumors are under-sampled in the clinic, such that only 0.0005% of initial tumor volume is used as input for diagnostic testing. Litchfield et al. apply the principles of representative sampling to implement an unbiased tumor sampling approach that improves the reproducibility and accuracy of next-generation sequencing.

Litchfield et al., 2020, Cell Reports *31*, 107550
May 5, 2020
https://doi.org/10.1016/j.celrep.2020.107550

CellPress

Cell Reports

CellPress
OPEN ACCESS

Resource

Representative Sequencing: Unbiased Sampling of Solid Tumor Tissue

Kevin Litchfield,[1,13] Stacey Stanislaw,[2,13] Lavinia Spain,[1,3] Lisa L. Gallegos,[2] Andrew Rowan,[1] Desiree Schnidrig,[1] Heidi Rosenbaum,[4] Alexandre Harle,[1,5] Lewis Au,[1,3] Samantha M. Hill,[2,6] Zayd Tippu,[3] Jennifer Thomas,[3] Lisa Thompson,[7] Hang Xu,[1] Stuart Horswell,[8] Aoune Barhoumi,[2] Carol Jones,[2] Katherine F. Leith,[2] Daniel L. Burgess,[4] Thomas B.K. Watkins,[1] Emilia Lim,[1] Nicolai J. Birkbak,[1,9] Philippe Lamy,[9] Iver Nordentoft,[9] Lars Dyrskjøt,[9] Lisa Pickering,[3] Stephen Hazell,[10] Mariam Jamal-Hanjani,[11,12] PEACE Consortium, James Larkin,[3] Charles Swanton,[1,11,12,*] Nelson R. Alexander,[2,*] and Samra Turajlic[1,3,14,*]

[1]Cancer Evolution and Genome Instability Laboratory, The Francis Crick Institute, 1 Midland Road, London NW1 1AT, UK
[2]Roche Tissue Diagnostics, 1910 E. Innovation Park Drive, Tucson, AZ 85755, USA
[3]Renal and Skin Units, The Royal Marsden Hospital, London SW3 6JJ, UK
[4]Roche Sequencing Solutions, Madison, 500 S. Rosa Road, Madison, WI 53719, USA
[5]Université de Lorraine, CNRS UMR 7039 CRAN, Institut de Cancérologie de Lorraine, Service de Biopathologie, 54000 Nancy, France
[6]Department of Cancer Biology, University of Arizona Cancer Center, Tucson, AZ 85724, USA
[7]The Centre for Molecular Pathology, The Royal Marsden Hospital, London SW3 6JJ, UK
[8]Department of Bioinformatics and Biostatistics, The Francis Crick Institute, London NW1 1AT, UK
[9]Department of Molecular Medicine, Aarhus University Hospital, Aarhus, Denmark
[10]Histopathology Department, Royal Marsden NHS Foundation Trust, London and Sutton, UK
[11]Cancer Research UK Lung Cancer Centre of Excellence, University College London Cancer Institute, London, UK
[12]Department of Medical Oncology, University College London Hospitals, London, UK
[13]These authors contributed equally
[14]Lead Contact
*Correspondence: charles.swanton@crick.ac.uk (C.S.), nelson.alexander@roche.com (N.R.A.), samra.turajlic@crick.ac.uk (S.T.)
https://doi.org/10.1016/j.celrep.2020.107550

SUMMARY

Although thousands of solid tumors have been sequenced to date, a fundamental under-sampling bias is inherent in current methodologies. This is caused by a tissue sample input of fixed dimensions (e.g., 6 mm biopsy), which becomes grossly under-powered as tumor volume scales. Here, we demonstrate representative sequencing (Rep-Seq) as a new method to achieve unbiased tumor tissue sampling. Rep-Seq uses fixed residual tumor material, which is homogenized and subjected to next-generation sequencing. Analysis of intratumor tumor mutation burden (TMB) variability shows a high level of misclassification using current single-biopsy methods, with 20% of lung and 52% of bladder tumors having at least one biopsy with high TMB but low clonal TMB overall. Misclassification rates by contrast are reduced to 2% (lung) and 4% (bladder) when a more representative sampling methodology is used. Rep-Seq offers an improved sampling protocol for tumor profiling, with significant potential for improved clinical utility and more accurate deconvolution of clonal structure.

INTRODUCTION

Over the past decade, clinical researchers have demonstrated the inability of an individual biopsy or formalin-fixed paraffin-embedded (FFPE) block to capture the genetic diversity of a solid tumor (Turajlic et al., 2018; Jamal-Hanjani et al., 2017; Warrick et al., 2019). This issue stems from the reliance on single-site samples, which are used as the current standard protocol for tumor sequencing in both research and clinical contexts. Sampling only once, from a single spatial location, will miss major expanding tumor subclones in other distant tumor locations, creating a bias that cannot be resolved through excess sequencing depth. Moreover, this widespread sampling bias is inherently obscured because the unsampled fixed tumor tissue not submitted for paraffin embedding is considered surgical waste and is incinerated. The pitfalls of using a non-representative sampling method are well documented in the "theory of sampling" developed by Pierre Gy (Gy, 1988) and have been practically demonstrated across multiple fields, ranging from food contamination to electoral polling and the mining industry (Rohde et al., 2015; Crespi, 1988; David, 1988). In the case of tumor sequencing, this bias arises within the context of spatially biased intratumor heterogeneity (ITH) as an important feature of cancer, combined with the increasing utility of molecular profiling as a tool to stratify patients for therapy (AACR Project GENIE Consortium, 2017). Failure to address this issue risks undermining the clinical utility of genomic medicine in cancer, through reduced sensitivity to detect prognostic and predictive markers, a lack

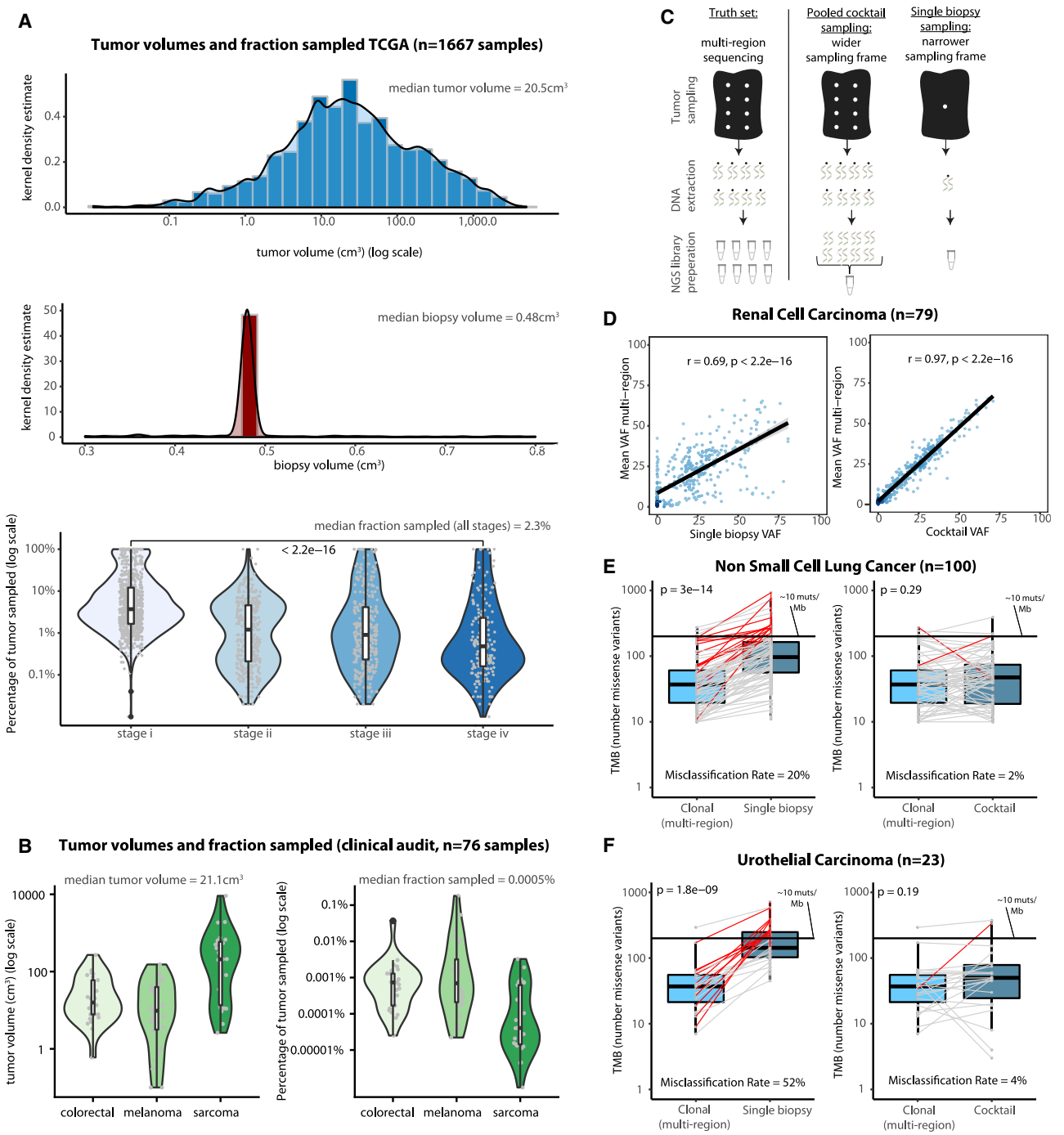

Figure 1. Current Tumor Sequencing Methods Lead to Under-sampling, Which Can Be Resolved through a Wider Sampling Frame

(A) Top: a density plot of the distribution of tumor volumes from The Cancer Genome Atlas (TCGA), with tumor volume (cubic centimeters) plotted on the x axis with log scale. Middle: a density plot of the volume of biopsy tissue used as input material for sequencing in the same cohort of TCGA samples. Bottom: the proportion of tissue sampled (i.e., values from the middle panel divided by those from the top panel for each case), split by tumor stage.

(B) Left: the estimated tumor volume (cubic centimeters) from a clinical audit, split by tissue site. Right: the proportion of tissue sampled, split by tissue site, in the clinical audit.

(C) The experimental design used for pilot experiment of pooled "cocktail" samples.

(D) Left: the variant allele frequency (VAF) correlation between cocktail sequencing (x axis) compared with true VAFs estimated from multi-biopsy sequencing (y axis); right: the variant allele frequency (VAF) correlation between single-region sequencing (x axis) compared with true VAFs estimated from multi-biopsy sequencing (y axis).

(legend continued on next page)

of reproducibility in sequencing results among samples, misassignment of subclonal variants as clonal (Pearson et al., 2016), and unreliable estimates of tumor mutation burden (TMB). A frequently proposed solution is to conduct multi-region sampling and profiling, which although able to address these issues in a research setting is cost prohibitive and too labor intensive for wide-scale adoption in clinical practice. Furthermore, the recurrent question of how many biopsies should be taken is unanswerable because of the high variability in ITH among patients (Turajlic et al., 2018). We hypothesized that a new sampling methodology could be implemented to circumvent these limitations, through the use of residual tumor tissue to create a more representative sample that captures the heterogeneity of the total tumor mass. We show that this new method better captures the diversity of the tumor and leads to improved biomarker results, without the need for increased sequencing depth or for multiple samples to be profiled per tumor. Furthermore, as the method described herein removes the physical bias of single-sample profiling and makes use of residual fixed tumor material that would otherwise be clinical waste, it empowers clinicians and researchers with a practical solution to overcome sampling bias within current tumor sequencing protocols.

RESULTS

Audit of Current Sampling Protocols

To examine the extent of current under-sampling bias in cancer genomics, we first analyzed pan-cancer sequencing data from The Cancer Genome Atlas (TCGA). Clinical annotation files were extracted for each solid tumor cohort from the Broad Institute's TCGA GDAC Firehose repository, from which tumor length and width data were available for 1,667 samples across six tumor types (STAR Methods). For each sample, total tumor tissue volume and research sample volume were estimated from the clinical data, and the two values were compared to assess the proportion of total tumor mass sampled for each case (STAR Methods). This revealed that current research protocols sample on average only 2.3% of the tumor mass (median value for all stages, n = 1,667 samples), decreasing to 0.5% for stage IV tumors (median value, n = 181) (Figure 1A). We next investigated this pattern within a routine clinical context, through audit of randomly selected cases undergoing molecular profiling as part of standard of care at a major cancer center (see STAR Methods). In total, 76 cases were audited, across three different solid tumor types. This revealed a median clinical tumor sampling proportion of only 0.0005% (range 0.000001%–0.2%) (Figure 1B), reflecting the minimal input material provided from standard FFPE tumor sections. The remaining $\geq$99.9% of tumor tissue is left unsampled for molecular profiling purposes, leading to a high level of under-sampling in a clinical context. Thus, within both research and clinical settings, current tumor sequencing protocols are associated with a high under-sampling bias. Furthermore, we note that sampling bias is also likely to be affected by the level of heterogeneity and the purity of tumor cells in the sample (Figure S1).

A More Representative Sample Leads to Increased Ability to Detect Variants and Improved Accuracy in TMB Estimation

To investigate the effect of spatial bias in single-biopsy sampling, we first conducted a pilot experiment, creating a single, more representative sample by pooling extracted DNA from 1,184 multi-region biopsies, taken from 79 primary renal cell carcinomas (RCCs), to create "cocktail" solutions per tumor (Figure 1C). Pooled cocktail samples were subject to next-generation sequencing (NGS) (median depth 674×), and mutation calls were compared with previously generated single-biopsy (reflecting current clinical practice; median depth 608×) and multi-region biopsy (truth set) data (median depth 612×) (Turajlic et al., 2018). Multi-region variant allele frequencies (VAFs) were determined by taking the mean across all regions per tumor, and single-region samples were selected by random sampling (see STAR Methods). All samples were processed through an identical protocol (see STAR Methods). Across all 79 tumors, the cocktail samples discovered a median of 100% (range 30%–100%) of the truth-set mutations compared with single biopsies, which achieved a median discovery rate of 73% (range 15%–100%), supporting the hypothesis that a more representative sample leads to improved ability to detect variants ($p = 6.6 \times 10^{-11}$, paired Wilcoxon test; Figure S2). In addition, VAFs derived from cocktail samples demonstrated a strong correlation with true VAF values from multi-region sequencing ($r = 0.97$), a superior correlation compared with that achieved by single-biopsy sampling ($r = 0.69$) (Figure 1D). This suggests that using a single, more representative sample provides a more accurate estimation of true cellular mutational prevalence across the total tumor mass (the true search space), an important consideration for both prognostic and predictive biomarkers. Within this context, TMB is emerging as a robust predictive biomarker for immune checkpoint inhibitor (CPI) therapy, validated across multiple tumor types (Forde et al., 2018; Hellmann et al., 2018; Snyder et al., 2014; Mariathasan et al., 2018). In particular clonal mutation load (clonal TMB) has been shown to be the key driver of CPI response (McGranahan et al., 2016; Miao et al., 2018), with subclonal mutations likely playing a neutral or negative role in achieving a sustained anti-tumor immune response (Gejman et al., 2018). To explore this further in the context of tumor sampling, we analyzed multi-region TRACERx non-small cell lung cancer (NSCLC) (Jamal-Hanjani et al., 2017) and urothelial carcinoma (UC) (Lamy et al., 2016; Thomsen et al., 2016) datasets and found high levels of intratumor TMB variability. In total, 20% of NSCLC cases (n = 100) and 52% of UC cases (n = 23) had one or more single biopsies with high TMB but low clonal TMB overall (on the basis of the prospectively validated 10.0

(E) Left: data from 100 non-small cell lung cancer cases, with clonal tumor mutation burden (TMB) values compared with single-biopsy TMB values (paired values within the same case are joined by gray line). Right: the same data, this time with clonal TMB compared with TMB estimates from *in silico* "cocktail" sampling. Red lines denote cases for which one paired value is below the 10 muts/Mb threshold and one is above. The 10 muts/Mb threshold is defined as 200 missense mutations.

(F) Urothelial carcinoma data from 23 patients, following the same format as (E).

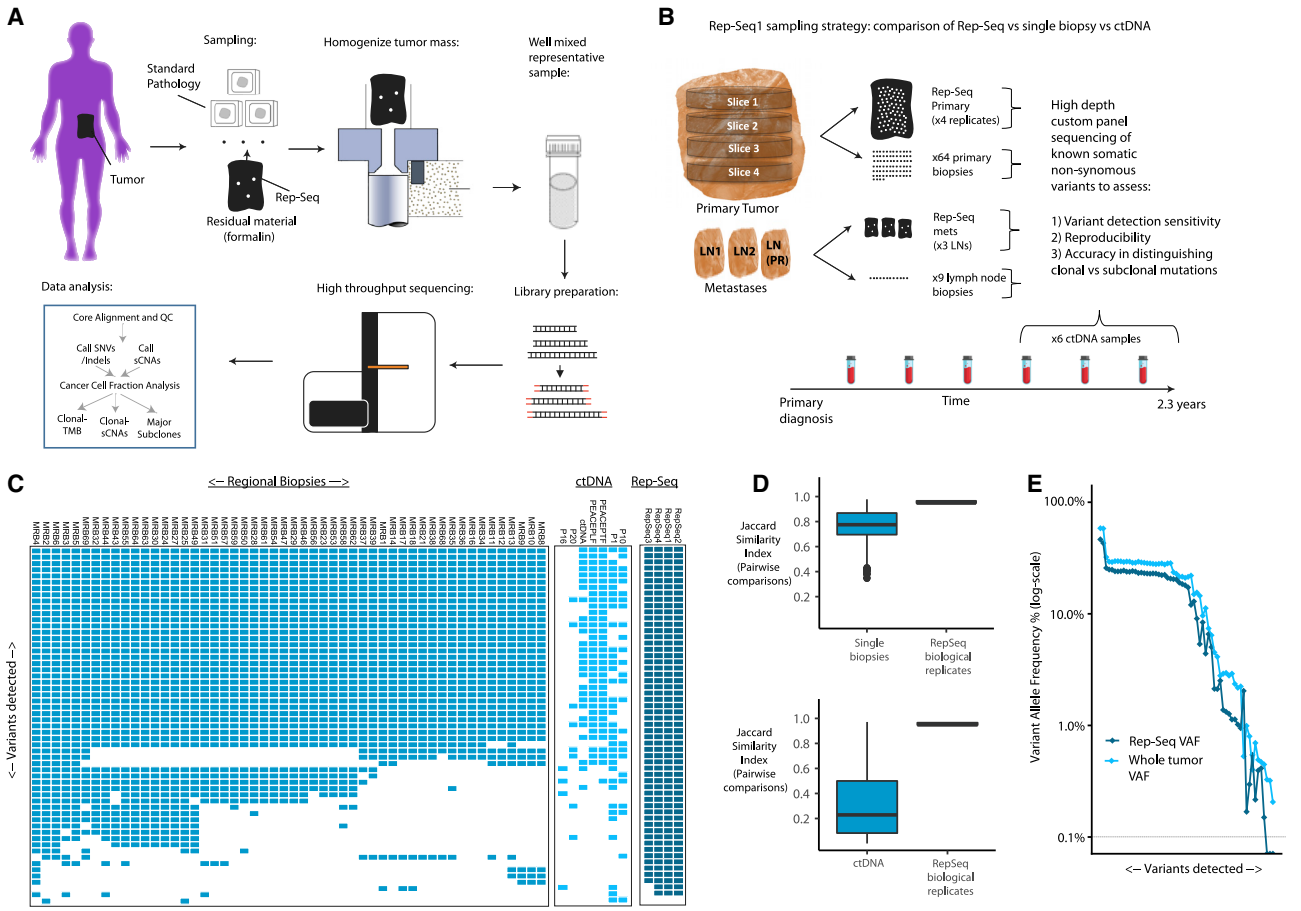

Figure 2. Representative Sequencing Method

(A) The methodological workflow for Representative Sequencing (Rep-Seq).

(B) The sampling strategy for case RS1, for validation of the Rep-Seq method against extensive biopsy sampling.

(C) The map of non-synonymous variants discovered in RS1, across tumor biopsies, ctDNA samples, and Rep-Seq biological replicates. PEACPLF is a cfDNA taken from pleural fluid, and PEACPTF is a cfDNA taken from peritoneal fluid, both at the time of rapid autopsy, and ctDNA is a pooled sample of P1/P10/P16/P20 timepoints.

(D) Jaccard similarity index results, as a measure of reproducibility, for single-biopsy sequencing versus Rep-Seq (left) and ctDNA sequencing versus Rep-Seq (right).

(E) The variant allele frequency (VAF) of mutations detected in RS1 Rep-Seq (dark blue) compared with VAF for the same mutation in the whole RS1 tumor (calculated as an average across all biopsies).

mutations/Mb threshold for CPI therapy; Forde et al., 2018; Figures 1E and 1F). These variability rates, in contrast, were reduced to 2% (NSCLC) and 4% (UC) when we generated *in silico* "cocktail" solutions and predicted clonal TMB (from the single cocktail sample; see STAR Methods), highlighting the potential clinical utility of a more representative sample in reducing the risk for TMB misclassification (Figures 1E and 1F). Finally, we assessed the ability of cocktail sequencing to determine clonal versus subclonal somatic copy number alterations (SCNAs), using the primary RCC dataset (n = 79). Known RCC clonal events (Turajlic et al., 2018) (e.g., loss of 3p25.3 and gain of 5q35.3) were found to have higher logR (log_2 ratio of coverage for tumor versus matched normal samples) than other (predominantly) subclonal alterations (Figure S2), indicating that clonal and subclonal SCNA events may be distinguishable in a pooled sequencing approach.

Homogenization of Residual Tumor Material to Create a Truly Representative Sample

Next, we next sought to develop an updated tumor sampling methodology that was consistent with the theory of sampling (Gy, 1988) and suitable for clinical adoption (i.e., not reliant on resource-intensive multiple-biopsy sampling and DNA extraction, as required for cocktail sampling). Here we demonstrate a new method called "representative sequencing" (Rep-Seq), which comprises homogenization of solid tumor masses into well-mixed solutions, coupled with NGS (Figure 2A). Tumor masses were sourced as the entire residual tumor material not taken for pathology assessment following surgery, material that would otherwise have been treated as clinical waste and destroyed (per College of American Pathologists and Royal College of Pathologists guidelines) or bio-banked. Residual samples represented on average 54.8% of the total tumor volume and

provided on average 223.5 g of tissue per tumor (on the basis of our pilot cohort of cases; see Table S1). These values are a significant increase over the average of 0.0005% sampled, and 0.0001 g of tumor tissue, currently used as sampling input in standard molecular profiling approaches. Following dissection of the formalin-fixed residual tumor tissue away from the surrounding normal tissue, the residual tumor mass is homogenized into a representative solution. From this well-mixed solution, samples are drawn for DNA extraction, library preparation, and sequencing (Figure 2A). Rep-Seq was implemented on a proof-of-concept basis in 11 tumors, from four different cancer types (Table S1).

Reproducibility and Sensitivity of Rep-Seq Compared with Biopsy Sequencing

The first tumor processed was RS1, a large clear cell RCC (ccRCC) tumor (17 cm maximal dimension), selected to allow extensive sampling for cross-validation purposes. In total, 64 fresh-frozen individual biopsies were taken from the primary tumor, and the remaining formalin-fixed residual mass (1,258 g of tissue) was homogenized under the Rep-Seq protocol. To define the variant landscape in this tumor, whole-exome sequencing (WES) was first conducted on a selection of 7 spatially disparate primary biopsies and an aliquot of the Rep-Seq sample (median depth 162×), leading to the discovery of a total of 76 non-synonymous mutations (single-nucleotide variants [SNVs] and small-scale insertion/deletions). These 76 mutations were subsequently captured in a targeted custom panel and successfully sequenced to high depth (median depth > 10,000×) in the 64 primary biopsies, 11 biopsies taken from two lymph node (LN) metastases, four separate aliquots drawn from the representative homogenate of the primary tumor sample (biological replicates), six circulating tumor DNA (ctDNA) samples collected at different time points, and three homogenized LN Rep-Seq samples (one LN was not biopsied) (Figure 2B). This integrated dataset was used to comprehensively evaluate the Rep-Seq methodology (Figure 2C). First we evaluated the reproducibility of each method, comparing the Jaccard similarity index between pairwise combinations of tumor biopsies, versus pairwise biological replicates of Rep-Seq, and pairwise combinations of ctDNA time points. Median pairwise similarity between biopsies was 0.78, suggesting that approximately 20–25% of mutations discovered in individual biopsies cannot be reproduced in subsequent biopsy samples. In contrast, median similarity among Rep-Seq replicates was higher at 0.95 (Figure 2D), with almost identical mutation lists discovered by each replicate (Figure 2C). Pairwise similarity among plasma ctDNA samples was low (overall median similarity index = 0.24; Figures 2C and 2D), reflecting the technical challenges of ctDNA profiling. The ongoing temporal evolution of the tumor across ctDNA time points should also be recognized, but we note substantial difference even among samples drawn close time points (e.g., P16 and P20 were only 21 days apart but shared no mutations in common). Last, we assessed the sensitivity of variant detection in case RS1 and note that variants as low as 0.15% VAF were successfully detected in the Rep-Seq sample (Figure 2E). In addition, the VAFs from Rep-Seq closely followed the overall tumor VAFs, as measured from the set of 64 biopsies (overall tumor VAF was calculated as total alt read count/total read count, summed across all biopsies) (Figure 2E). Only 3 mutations (of the 76 captured) were not detectable in the Rep-Seq sample, all with VAFs below 0.3%, close to the technical limit of ~0.1% VAF for variant detection using NGS protocols.

Clonal Structure Prediction from Rep-Seq Compared with Biopsy Sequencing

Next, we investigated the utility of Rep-Seq in determining clonal structure, given that measures of clonal diversity have been shown to associate with prognosis (Turajlic et al., 2018; McGranahan et al., 2016). Cancer cell fraction (CCF) estimates were first calculated for all mutations (n = 76) within the RS1 primary tumor biopsy set (n = 52 biopsies used, n = 12 excluded because of low purity; see STAR Methods) and grouped together into mutational clusters to infer a high-confidence benchmark clonal structure. Four distinct tumor clones were detected: clone A (truncal clone, mutations in every cancer cell, CCF = 100.0%, n = 41 mutations) and (sub)clones B (CCF = 45.6%, n = 2 mutations, and 14q loss as a known RCC driver SCNA event; Turajlic et al., 2018), C (CCF = 52.8%, n = 6 mutations), and D (CCF = 17.1%, n = 2 mutations) (Figure 3A). The remaining mutations were predominantly lower frequency and could not be reliably clustered into subclones. The clustering process was repeated for the Rep-Seq sample alone (n = 1), and the clonal solution was then compared between methods (Figure 3A). Rep-Seq correctly clustered all 41 clonal mutations together into truncal clone A (CCF = 100.0%), as well as identifying two major (sub) clones, B (CCF = 40.6%) and C (CCF = 33.3%) (Figure 3A) (we note that the sets of mutations in subclones B and C were not fully identical between the multi-region and Rep-Seq solutions). The remaining mutations in the Rep-Seq sample were again predominantly lower frequency and could not be reliably clustered, reflecting the challenge in accurately grouping together low-CCF mutations. CCF estimates from both methods were validated against physical mapping of spatial biopsy locations and mutational presence back to images of the sampled tumor: (sub)clone B was found in 20 of 52 primary biopsies (38.4%), and (sub)clone C was found in 32 of 52 (61.5%) (Figure 3B). This confirmed the presence of two major, spatially distinct subclones. Intriguingly, LN metastases LN1 and LN2 were exclusively seeded by clone B, whereas spatially proximal peri-renal LN sample LN(PR) was polyclonal, with clones B and C present. Individual mutation CCFs within each sample were next considered, in order to assess how well separated truncal events (clone A) were from subclonal mutations (clones B and C). Within the Rep-Seq sample, CCF estimates for clonal events (clone A) were clearly separated from (sub)clones B and C, reflecting the rapid convergence of CCF estimates in Rep-Seq toward true values (Figure 3C, right). In contrast, CCF distributions in single-sample biopsies overlapped among clones A, B, and C, with sub(clones) B and C frequently appearing (incorrectly) as clonal in individual biopsies with CCFs of ~100% (“illusion of clonality”; Burrell and Swanton, 2016). On average across the 52 primary biopsies, 17% (range 6%–35%) of clonal variants suffered from an illusion of clonality, if they were considered a single-region sample (Figure 3D) (all 76 mutations included; see STAR Methods). An illusion of clonality persisted even with multi-region biopsy

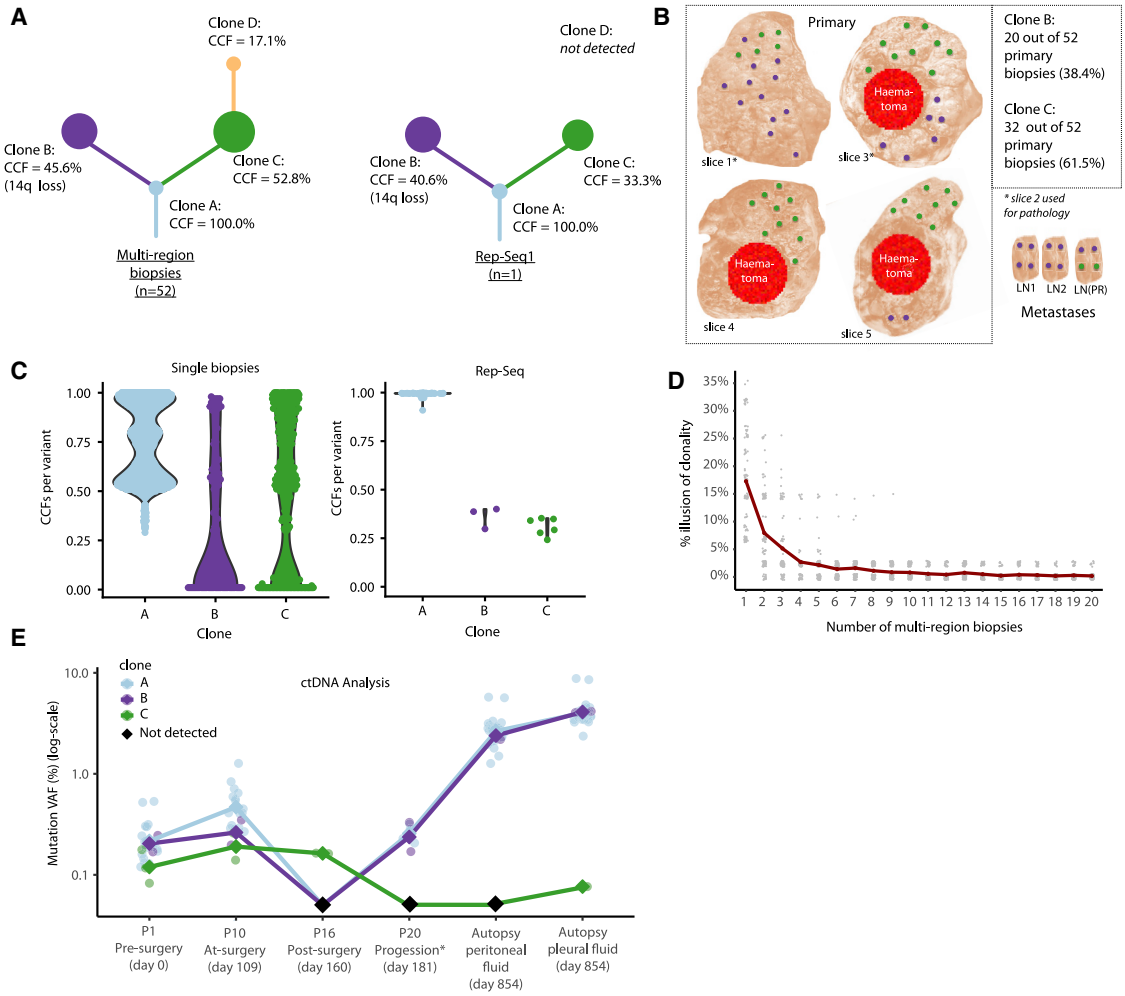

Figure 3. Clonal Tracking by Rep-Seq and ctDNA in Renal Cell Carcinoma

(A) The phylogenetic tree for case RS1, as derived using extensive multiple-biopsy sequencing (left) and a single Rep-Seq sample.

(B) The clonal distribution across the four slices of the primary RS1 tumor and lymph node metastases.

(C) The cancer cell fraction (CCF) estimates for mutations in tumor clones A, B, and C in each biopsy sample (left) and in the Rep-Seq sample (right).

(D) The illusion of clonality simulation data, with the number of simulated biopsy samples plotted on the x axis and the percentage of variants that incorrectly appear to be clonal (illusion of clonality) on the y axis (from 100 simulated sample combinations).

(E) ctDNA data for RS1, with the VAFs plotted (y axis) for mutations in clones A, B, and C.

sampling, with simulation showing that two random biopsies yielded an illusion of clonality rate of 9% (range 0%–25%), three of 6% (range 0%–25%), four of 4% (range 0%–15%), and five of 3% (range 0%–15%) (Figure 3D). Furthermore these results are likely to represent a conservative under-estimation of true illusion of clonality rates, as 3-dimensional sampling was conducted along the z axis in this case. We note that if standard 2-dimensional tumor slice sampling had been conducted only on slice 4, which was monoclonal for clone C, no number of biopsies would have prevented clonal illusion (Figure 3B), and critically, clone B (which metastasized to the LNs) would have been completely missed.

Given the broad applicability of liquid biopsies, and previous work demonstrating that both clonal and subclonal mutations can be identified (Abbosh et al., 2017), a pertinent question is to what extent ctDNA samples from plasma represent true clonal diversity compared with a more representative sampling of the primary tumor. Taking advantage of a well-characterized primary tumor, and five longitudinal ctDNA time points, we investigated this question. At pre-surgery time points (P1 and P10), variants from clones A, B, and C were all detectable at VAFs of 0.1%–1.0%, but many variants were missed, including some clone A truncal events, reflecting the technical challenges of profiling ctDNA. Mean VAF within clone A was overall higher than within (sub)clones B and C, but large inconsistency was observed in terms of individual variants analyzed across time points (Figure 3E). At post-surgery time point P16, the highest VAF variant was from clone C, and similarly at time point P20, a clone B mutation was highest, both above any clone A truncal mutations (Figure 3E). At later stage time points, however (post-mortem

sampling), all clonal mutations were detected, with highly consistent VAF frequency (Figure 3E). Correlation coefficients of VAFs from ctDNA, compared with the count of how many biopsies a mutation was present in, ranged from r = −0.17 (time point P16) to r = 0.78 (pleural fluid obtained post-mortem). Rep-Seq CCFs had the highest correlation with biopsy count data (r = 0.90). This suggests that inferring *de novo* clonal structure from ctDNA alone remains challenging, but tracking clonal markers that have been previously identified from tumor tissue remains highly informative (e.g., for minimal residual disease [MRD] tracking). We note, in the context of MRD tracking, that a larger panel of variants is likely to increase sensitivity to detect relapse at earlier time points (e.g., in the RS1 data at time point p16, an MRD panel based on mutations from a single biopsy would have missed disease relapse 53% of the time, compared with a 0% miss rate using a Rep-Seq-based panel; Table S2). In terms of the clonal dynamics of RS1, an interesting pattern was observed, with clone C dying out at later ctDNA time points and becoming undetectable (Figure 3E). This supports the predicted metastatic seeding pattern, as determined by biopsy and Rep-Seq profiling, that is, that clone B achieved distal metastatic seeding, whereas clone C was contained within the (peri-)renal area (Figure 3B). As an additional validation, copy number analysis was conducted on 31 further biopsies sampled from 20 distinct anatomical sites of metastatic disease present at the time of RS1 autopsy. All sites contained loss of 14q, a driver event found only in clone B in the primary tumor (Figure S3). We note that in single-region biopsy sequencing, metastasizing clone B would have been missed 32 times out of 52 (61.5%).

Rep-Seq Implemented on Lymph Node Samples in the Context of Metastatic Melanoma

To understand the utility of Rep-Seq profiling on LN residual material (as opposed to RS1, for which a large primary tumor was also available), we homogenized two LN samples (internal iliac LN and right inguinal LN) from a patient with metastatic melanoma (case RS2). In parallel, single-biopsy LN (right inguinal LN) sequencing was additionally conducted (biopsy taken prior to homogenization), as well as multi-region biopsies sequenced from a further eight distinct anatomical sites of metastases, in order to validate the Rep-Seq methodology (total n = 17 samples). All samples underwent WES (median coverage ~200×), with tissue sampled at the time of rapid autopsy (STAR Methods). The first question was to compare the results from LN Rep-Seq with those from single-sample LN sequencing, which would be the standard sampling approach in the context of a LN dissection. CCF clustering analysis was completed for the LN single sample (see STAR Methods; Figure 4A), and the calculated tree was monoclonal in structure (100% of mutations were predicted clonal, n = 90). Results from the homogenized Rep-Seq LN sample, in contrast, calculated a polyclonal tumor structure, with only 63% of mutations (n = 58) being clonal and the remaining mutations (n = 34) being subclonal, clustered into four distinct subclones (Figures 4B and 4C). To verify which solution was correct (mono- versus polyclonal), a joint clustering analysis was completed across all biopsy samples (n = 16 from LN and eight distal metastases) to yield a high-confidence clonal solution (Figure 4D). The tumor was indeed found to be polyclonal, with a total of seven distinct tumor subclones detected (Figure 4D). A major branch encompassing multiple distinct subclones (Figure 4D, far left of tree) was found to be shared across pelvic, liver, paravertebral, abdominal wall, loin soft tissue, and supra-renal metastases but was absent in two distinct right groin soft tissue masses (Figure 4D). The right groin masses were each characterized by distinct tumor subclones (Figure 4D). A number of individual sites were also found to be polyclonal in nature (e.g., liver, paravertebral mass) containing both the major left-hand subclone branch and the distinct subclones present in the right groin masses (Figure 4D). These polyphyletic patterns would be consistent with either polyclonal dissemination from the primary or metastasis-to-metastasis seeding. We note that not all tumor subclones were detectable using the Rep-Seq LN methodology, but the representative sampling methodology was accurate enough to clearly distinguish this as a polyclonal tumor, with a lower proportion of mutations being clonal. This finding was supported by extensive sampling of multiple metastases. The single-site sample, in contrast, incorrectly predicted a monoclonal tumor structure, with all mutations being clonal in nature. Clinically, we note that this patient received three lines of immune CPI therapy (adjuvant nivolumab, ipilimumab, and pembrolizumab) and failed to respond throughout, with progressive disease recorded for all rounds and sites of CPI treatment (Figure 4E). Although only descriptive in nature, this lack of response would be consistent with the hypothesis of a heterogeneous subclonal neoantigen repertoire being associated with poor response to immunotherapy (Wolf et al., 2019). For completeness, we additionally obtained archival FFPE blocks for the RS2 primary tumor sample, and at median ~200× sequencing coverage, none of the metastasizing clones were detectable, highlighting the challenge of melanoma primary tissue sampling where the tumor size is so small.

Rep-Seq Implemented on an Extended Cohort of Primary Solid Tumors across Four Tissue Types

The Rep-Seq method was additionally conducted in a further ten cases as a technical feasibility exercise. Cases RS3 and RS4 were ccRCC tumors and predominantly monoclonal in structure (Figure S4). Cases RS5–RS11 were tumors of breast, colorectal, and lung origin, and tumor-specific driver mutations were successfully detected in all specimens (Table S3). The highest mutation burden was observed in RS8 (colon), with 980 and 251 non-synonymous SNVs and indels and presence of cosmic mutational signatures 6 and 15 associated with mismatch repair deficiency (Figure 5A), which was confirmed by immunohistochemistry staining showing loss of *MLH1*. Signature analysis of the three NSCLC tumors (RS9, RS10, and RS11) showed evidence of signature 4 (smoking associated) uniquely in these three tumors only (Figure 5A). Hence the mutational signatures derived from Rep-Seq were consistent with expected patterns.

Tumor Purity-Enriched Rep-Seq Protocol

Finally, an additional benefit of tissue homogenization is the preservation of the cellular integrity of the tissue and therefore the ability to add a cell-sorting step prior to DNA purification, to enrich for higher tumor purity. As a proof of principle, flow sorting was conducted on RS12 (colorectal tumor), preferentially selecting isolated tumor nuclei on the basis of the presence of

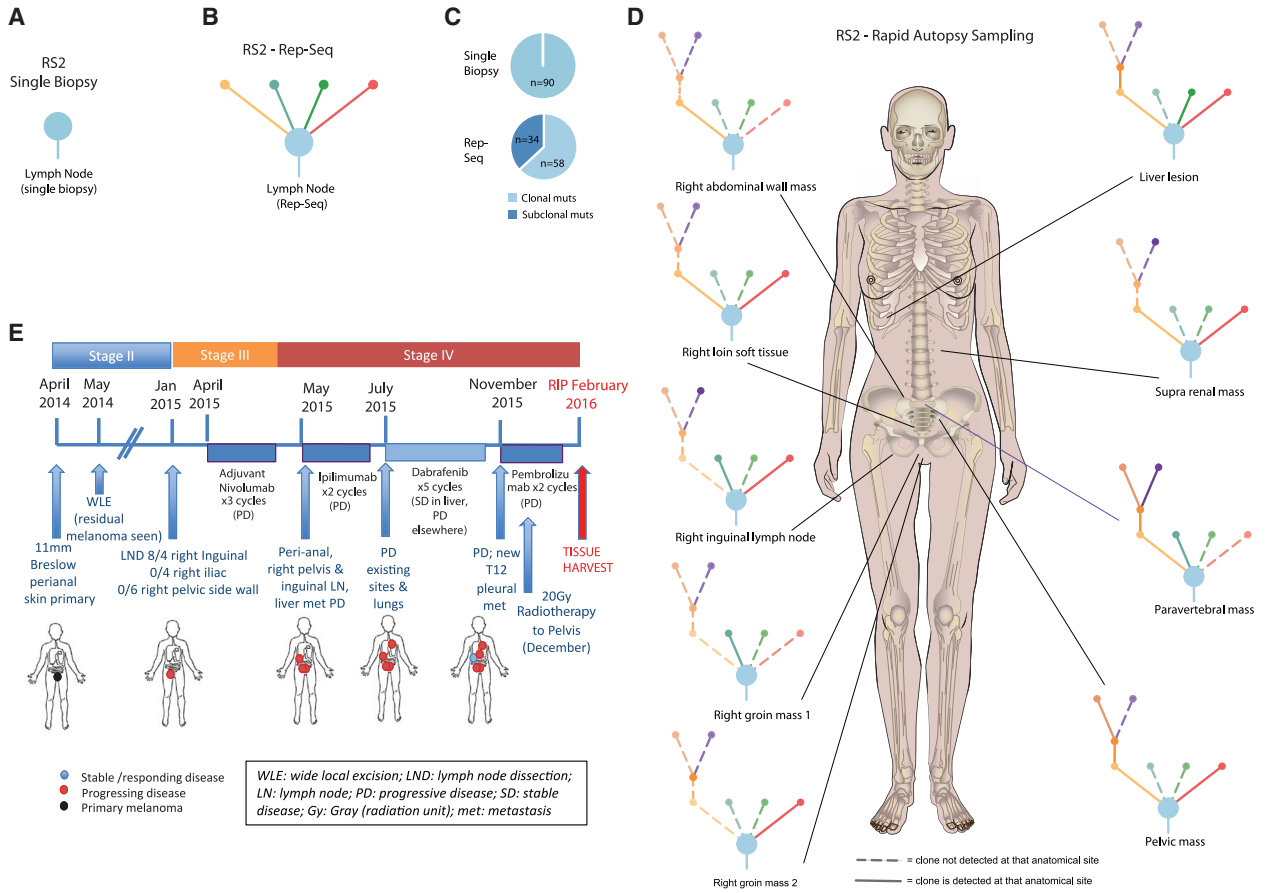

Figure 4. Clonal Tracking by Rep-Seq in Metastatic Melanoma

(A) The phylogenetic tree for case RS2 using single-biopsy lymph node sequencing (right inguinal LN).

(B) The phylogenetic tree for case RS2 using Rep-Seq LN sequencing.

(C) The proportion of mutations, clonal and subclonal, in RS2 on the basis of single-biopsy (top) and Rep-Seq (bottom) profiling.

(D) The extended phylogenetic tree for case RS2, on the basis of joint clustering of LN and eight distal metastases samples. Clone presence is marked on the basis of anatomical site of disease, with absent clones in a given site shaded in lighter color. Note that the right inguinal LN now becomes subclonal in composition, because of the benefit of multi-region joint clustering. Previously in (A), these same mutations are incorrectly clustered to the truncal clone (illusion of clonality) because of the limitations of single-biopsy sampling.

(E) The clinical history of case RS2. The best response by RECIST version 1.1 criteria is denoted in parentheses. SD, stable disease; PD, progressive disease.

cytokeratins 8 and 18 and high forward/side scattering. WES was conducted, first on a standard sample from the Rep-Seq protocol (non-sorted Rep-Seq, depth 221×), which showed tumor purity of 0.44. Strong enrichment was observed in the flow-sorted Rep-Seq sample (depth 215×), with purity of 0.89, which resulted in an approximate doubling of the effective tumor cell sequencing coverage (from 90× to 184×), for the same overall bulk sample sequencing depth and cost (Figure 5B). In terms of variant discovery, 365 non-synonymous SNVs were observed in common between both standard and flow-sorted samples, and then an additional 68 mutations (an increase of 19%) were found uniquely in the flow-sorted sample, presumably because of the increased sensitivity from higher effective tumor depth (Figure 5B). Only 5 mutations (1.4% of the total, all with VAFs < 5%) were found with the opposite pattern (i.e., in the standard sample but missing in the flow-sorted sample), which suggests in this case that flow sorting did not create systematic bias such that certain tumor subclones are excluded. The additional sensitivity in mutation detection enabled a larger set of subclones to be defined (Figure 5C).

DISCUSSION

Here we present Rep-Seq as a new method to achieve unbiased tumor sampling, drawing DNA molecules from a well-mixed homogenized solution of all residual surgical tumor material. This method removes the spatial bias inherent in current single-biopsy approaches and significantly increases the probability of detecting the genomic heterogeneity of solid tumors in a single sample protocol. Successful delivery of precision medicine in oncology is contingent on a reliable identification of biomarkers. ITH affects the interpretation of prognostic biomarkers and predictive biomarkers of response to targeted and immunotherapy, most notably TMB. Rep-Seq offers a clear opportunity to

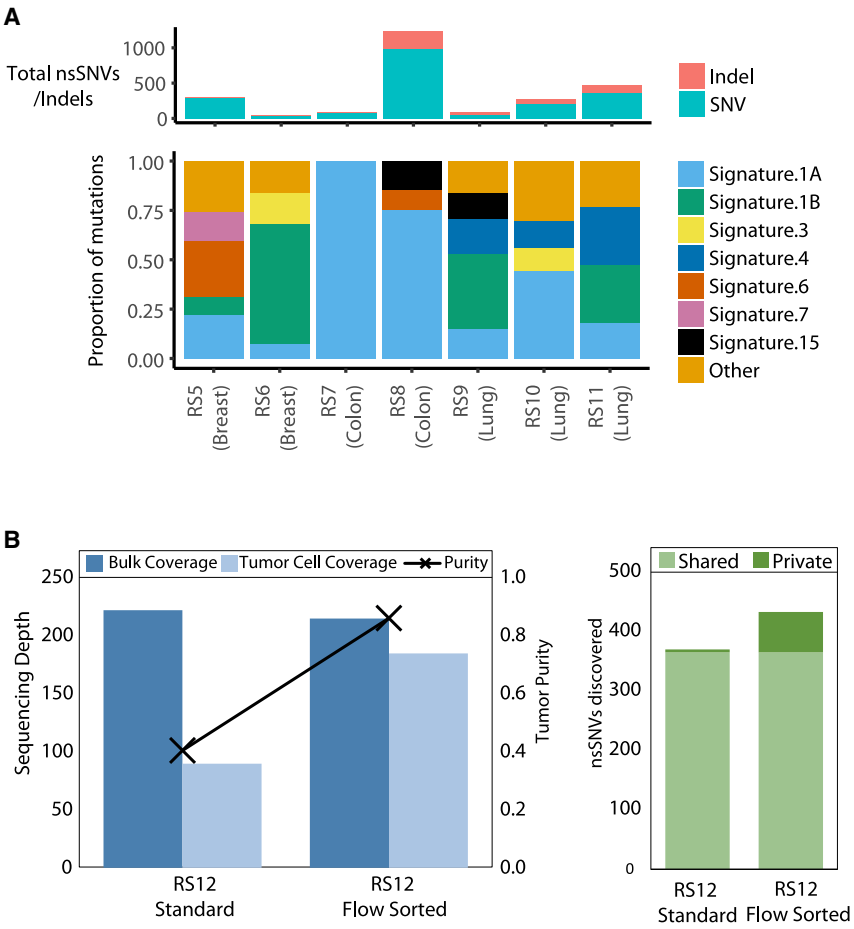

Figure 5. Extended Rep-Seq Cohort and Tumor Purity Enrichment

(A) Non-synonymous mutation count for cases RS5–RS11 (top), along with mutational signature analysis results (bottom).

(B) Left: RS12 coverage data for the overall bulk mixed cell population and then an estimated tumor cell coverage, along with purity estimates. Data are shown for standard Rep-Seq, and then tumor purity-enriched Rep-Seq, for comparison purposes. Right: the number of non-synonymous variants detected in normal and purity-enriched Rep-Seq samples. Variant counts are color coded on the basis of either being "shared" (i.e., present in both samples) or "private" (i.e., variant is present in only that sample and absent from the other).

(C) Phylogenetic trees for the normal and flow-sorted RS12 tumor subclones.

overcome the issue of ITH in these contexts and could feasibly be adopted in routine clinical practice.

In our analysis we first show the extent of under-sampling in current research studies, with data from TCGA demonstrating an average tissue sampling proportion of 2.3%. This bias is even more pronounced in a routine clinical context, with our audit data from standard molecular profiling at a major cancer center demonstrating that only five cancer cells in every million (0.0005%) are being sampled. This rate of under-sampling raises the risk for misinterpreting clinically relevant tumor sequencing results, as demonstrated by a high level of variability in TMB scores between single sites and the true clonal mutation load. Indeed, in NSCLC and UC, we show that 20% and 52% of cases, respectively, have at least one biopsy classified as high TMB, when the overall clonal TMB is low. This misclassification risk can be reduced through using a more representative sample, with discordance rates being reduced to 2% and 4%, respectively, using *in silico* "cocktail" analysis. We note, however, that the *in silico* "cocktail" samples may have slightly higher tumor purity than the main Rep-Seq methodology, as the latter takes all residual tumor material as input rather the biopsy-sampled regions.

To address the issue of spatial sampling bias in a manner consistent with the theory of sampling, as well as the challenge of multiple-biopsy sampling being too labor intensive for routine clinical use, we next sought to develop an updated tumor sampling methodology. We demonstrate Rep-Seq as a new method able to overcome both these points, through sampling a large volume of tumor tissue (average sampled proportion 55%), but maintaining a single (n = 1) DNA sample for downstream NGS library preparation and sequencing. The source of material in Rep-Seq is unique by making use of excess residual tumor tissue from surgery, which would otherwise be destroyed as clinical waste or bio-banked for research use. Homogenization of this residual tissue makes an ideal source for DNA extraction and sequencing, given the more representative nature of the sample, and generates a substantial amount of material that can be retained for future

research use. Such practices of homogenized sampling have been in routine practice in other fields for many decades, such as the sampling of mineral deposits. This fact, combined with the large amount tissue processed as clinical waste, highlights the sub-optimal nature of current molecular profiling sampling approaches in oncology. Here we demonstrate the utility of Rep-Seq through extensive sampling in a cohort of pilot cases, primarily as a proof-of-concept study. We show that the reproducibility in variant detection between replicates in Rep-Seq is high (Jaccard similarity index = 0.95) and superior to that of single-biopsy sequencing (0.78). In case RS1, sampling of >50 biopsies, from five tumor slices, validated the accuracy of Rep-Seq clonality predictions. In contrast, single-biopsy sequencing suffered from a high rate of illusion of clonality, with 17% of mutations appearing clonal when in reality they were subclonal. Conversely, single-biopsy sequencing also frequently missed important events, with 62% of biopsies missing the metastasizing clone. And notably all biopsies from tumor slice 4 missed the lethal clone, indicating that even extensive multi-region sampling is still susceptible to spatial bias, unless implemented on a 3-dimensional basis. Ultimately, any biopsy-based sequencing approach will retain spatial bias to some degree when tumor tissue is left unsampled, which hence emphasizes the benefit of a homogenization-based sampling approach.

In case RS2, we used Rep-Seq to profile LN metastases from a patient with primary melanoma, which revealed polyclonal disease. This was confirmed by extensive biopsy sequencing of eight further sites of distal metastases, which validated polyclonality, with multiple distinct subclones present across anatomically separate sites. Results from single-biopsy LN sequencing, in contrast, predicted a monoclonal tumor, which was shown to be incorrect. With increasing evidence now supporting clonal neoantigens as a key driver of immunotherapy response (Miao et al., 2018; Gejman et al., 2018), the accurate delineation of clonal versus subclonal alterations is of clinical relevance. This is descriptively illustrated in case RS2, in which lack of response to three lines of immunotherapy was observed, in the context of a high subclonal neoantigen repertoire. We additionally implemented Rep-Seq on a further ten cases (RS3–RS12), from lung, colorectal, and breast cancer types, showing mutation rates and signatures in line with expected results. Finally, as a further extension of the Rep-Seq protocol, we demonstrate flow sorting as a method to achieve tumor purity enrichment. For case RS12, purity was increased from 44% to 89%, with no observed shift or bias introduced to the sequencing results. Purity enrichment complements well the homogenization-based Rep-Seq approach and could significantly reduce sequencing costs (the same equivalent coverage of tumor cells could have been achieved in half the cost for case RS12).

We acknowledge small cohort size as a limitation of this work and confirm that a larger prospective study of Rep-Seq (n = 500 cases) is under way (ClinicalTrials.gov identifier NCT03832062). In addition, although Rep-Seq yields accurate and unbiased estimates of clonal and major subclonal mutations, this comes with the trade-off of losing resolution to detect lower frequency tumor (sub)clones. This trade-off may be acceptable in a clinical context, in which lower frequency mutations may be less directly actionable than widely expanded clonal or major subclonal driver events. Furthermore, we show with deep custom panel sequencing in case RS1 that low-frequency mutations can be reliably detected in Rep-Seq down to 0.3% VAF, with sensitivity determined by current limits in NGS accuracy. As more sensitive sequencing assays (e.g., duplex sequencing) become adopted, it is likely that Rep-Seq can be used to search for ultra-low-frequency events. We also acknowledge that Rep-Seq will not be applicable in all patient contexts, for example, patients with advanced-stage disease who undergo only biopsy sampling (no other surgeries). However, in metastatic cases undergoing resection, as well as primary surgery, there is broad potential for bio-banking and homogenization of residual material using the Rep-Seq approach. Finally, there is also potential scope for hybrid approaches, in which a large part of the residual material is homogenized, but then a portion (e.g., a transverse section) is also retained for spatially dependent analysis (e.g., imaging, spatial transcriptomics).

In summary, here we implement Rep-Seq as a new tumor sampling methodology combined with NGS, which adopts a more representative sampling approach via homogenization of residual tumor tissue. This method offers a clinically practical solution to the dramatic under-sampling bias inherent in current molecular profiling workflows. We find the reproducibility of results in Rep-Seq to be significantly higher than for current single-biopsy sequencing approaches (at same equivalent sequencing depth), and greater accuracy was also achieved in determining clonal from subclonal variants. We note that these results are predicted from the theory of sampling, a statistically driven rule set for sampling solid masses that are heterogeneous. These results offer potential clinical utility in the context of both prognostic (e.g., greater sensitivity to detect metastasis driving subclones) and predictive biomarkers (e.g., improved clonal TMB estimates).

STAR★METHODS

Detailed methods are provided in the online version of this paper and include the following:

- KEY RESOURCES TABLE
- LEAD CONTACT AND MATERIALS AVAILABILITY
- EXPERIMENTAL MODEL AND SUBJECT DETAILS
  - Clinical studies
- METHOD DETAILS
  - Clinical audit of current molecular profiling practices
  - Regional biopsy and cocktail sample preparation
  - Grossing and homogenization of residual tumor tissue
  - Genomic DNA purification from tissue and cfDNA
  - Target-enriched NGS Library construction and sequencing
  - Flow sorting method to increase tumor purity
- QUANTIFICATION AND STATISTICAL ANALYSIS
  - Tumor volume sampling analysis
  - Processing of sequencing data
  - Analysis of pooled cocktail sequencing data
  - Analysis of in-silico pooled cocktail sequencing data

SUPPLEMENTAL INFORMATION

Supplemental Information can be found online at https://doi.org/10.1016/j.celrep.2020.107550.

CONSORTIA

The members of PEACE Consortium are Chris Abbosh, Kai-Keen Shiu, John Bridgewater, Daniel Hochhauser, Martin Forster, Siow-Ming Lee, Tanya Ahmad, Dionysis Papadatos-Pastos, Sam Janes, Peter Van Loo, Katey Enfield, Nicholas McGranahan, Ariana Huebner, Sergio Quezada, Stephan Beck, Peter Parker, Henning Walczak, Tariq Enver, Rob Hynds, Mary Falzon, Ian Proctor, Ron Sinclair, Chi-wah Lok, Zoe Rhodes, David Moore, Teresa Marafioti, Elaine Borg, Miriam Mitchison, Reena Khiroya, Giorgia Trevisan, Peter Ellery, Mark Linch, Sebastian Brandner, Crispin Hiley, Selvaraju Veeriah, Maryam Razaq, Heather Shaw, Gert Attard, Mita Afroza Akther, Cristina Naceur-Lombardelli, Lizi Manzano, Maise Al-Bakir, Simranpreet Summan, Nnenna Kanu, Sophie Ward, Uzma Asghar, Emilia Lim, Faye Gishen, Adrian Tookman, Paddy Stone, Caroline Stirling, Andrew Furness, Kim Edmonds, Nikki Hunter, Sarah Sarker, Sarah Vaughan, Mary Mangwende, Karla Pearce, Lavinia Spain, Scott Shepherd, Haixi Yan, Ben Shum, Eleanor Carlyle, Steve Hazell, Annika Fendler, Fiona Byrne, Nadia Yousaf, Sanjay Popat, Olivia Curtis, Gordon Stamp, Antonia Toncheva, Emma Nye, Aida Murra, Justine Korteweg, Nahid Sheikh, Debra Josephs, Ashish Chandra, James Spicer, Ula Mahadeva, Anna Green, Ruby Stewart, Lara-Rose Iredale, Tina Mackay, Ben Deakin, Debra Enting, Sarah Rudman, Sharmistha Ghosh, Lena Karapagniotou, Elias Pintus, Andrew Tutt, Sarah Howlett, Vasiliki Michalarea, James Brenton, Carlos Caldas, Rebecca Fitzgerald, Merche Jimenez-Linan, Elena Provenzano, Alison Cluroe, Grant Stewart, Colin Watts, Richard Gilbertson, Ultan McDermott, Simon Tavare, Emma Beddowes, Patricia Roxburgh, Andrew Biankin, Anthony Chalmers, Sioban Fraser, Karin Oien, Andrew Kidd, Kevin Blyth, Matt Krebs, Fiona Blackhall, Yvonne Summers, Caroline Dive, Richard Marais, Fabio Gomes, Mat Carter, Jo Dransfield, John Le Quesne, Dean Fennell, Jacqui Shaw, Babu Naidu, Shobhit Baijal, Bruce Tanchel, Gerald Langman, Andrew Robinson, Martin Collard, Peter Cockcroft, Charlotte Ferris, Hollie Bancroft, Amy Kerr, Gary Middleton, Joanne Webb, Salma Kadiri, Peter Colloby, Bernard Olisemeke, Rodelaine Wilson, Ian Tomlinson, Sanjay Jogai, Christian Ottensmeier, David Harrison, Massimo Loda, Adrienne Flanagan, Mairead McKenzie, Allan Hackshaw, Jonathan Ledermann, Abby Sharp, Laura Farrelly, and Hayley Bridger.

ACKNOWLEDGMENTS

We greatly thank the staff at the Royal Marsden Pathology Lab for their kind collaboration and efforts to support this project, as well as the Renal and Skin Unit Research Team, also at the Royal Marsden NHS Foundation Trust. We gratefully acknowledge all members of the PEACE Consortium. We kindly thank Melinda Day and Patrick Brunhoeber for their early collaboration and support on this project, and we thank Joe Brock for his excellent illustration utilised in Figure 4. We dedicate this work to the memory of Martin Gore. Funding for this study was provided by Roche Tissue Diagnostics. K.L. is funded by the Medical Research Council (MR/P014712/1), the Rosetrees Trust (A2437), Cancer Research UK (C69256/A30194), and the CRUK Lung Cancer Centre of Excellence. A.H. is funded by Fondation de France. C.S. is a Royal Society Napier Research Professor. This work was supported by the Francis Crick Institute, which receives its core funding from Cancer Research UK (FC001169, FC001202), the Medical Research Council (FC001169, FC001202), and the Wellcome Trust (FC001169, FC001202). C.S. is funded by Cancer Research UK (TRACERx, PEACE, and CRUK Cancer Immunotherapy Catalyst Network), the CRUK Lung Cancer Centre of Excellence, the Rosetrees Trust, the NovoNordisk Foundation (ID16584), and the Breast Cancer Research Foundation (BCRF). This research is supported by a Stand Up To Cancer (SU2C)-LUNGevity-American Lung Association Lung Cancer Interception Dream Team Translational Research Grant (SU2C-AACR-DT23-17). SU2C is a program of the Entertainment Industry Foundation. Research grants are administered by the American Association for Cancer Research, the scientific partner of SU2C. C.S. receives funding from the European Research Council (ERC) under the European Union's Seventh Framework Programme (FP7/2007-2013) Consolidator Grant (FP7-THESEUS-617844), European Commission ITN (FP7-PloidyNet 607722), an ERC Advanced Grant (PROTEUS) from the ERC under the European Union's Horizon 2020 research and innovation program (835297), and Chromavision from the European Union's Horizon 2020 research and innovation program (665233). J.L. is supported by the National Institute for Health Research (NIHR) RM/ICR Biomedical Research Centre for Cancer. S.T. is funded by Cancer Research UK (C50947/A18176), the NIHR Biomedical Research Centre at the Royal Marsden Hospital and Institute of Cancer Research (A109), the Kidney and Melanoma Cancer Fund of The Royal Marsden Cancer Charity, the Rosetrees Trust (A2204), and Ventana Medical Systems Inc. (10467 and 10530). We thank the patients and their families.

AUTHOR CONTRIBUTIONS

Study Design, N.R.A., S.T., and C.S.; Laboratory Experiments, S.S., A.R., H.R., L.G., S. Hill, A.H., and D.L.B.; Clinical/Pathology Work, S.T., L.S., L.A., J.T., L.T., C.J., S. Hazell, and J.L.; Data Analysis, K.L., H.X., D.S., and S. Horswell; Data Interpretation, all authors; Manuscript Writing, K.L., S.T., N.R.A., S.S., H.R., L.G., and S.H.

DECLARATION OF INTERESTS

S.T. reports grants from Roche Tissue Diagnostics. K.L., S.T., and C.S. report speaker fees from Roche Tissue Diagnostics. K.L., S.S., S.T., and N.R.A. report a patent pending using Rep-Seq profiling to support detection of MRD. N.R.A., S.S., L.G., A.B., K.F.L., and S.H. have patents pending on representative sampling of solid tumors. C.S. receives grant support from Pfizer, AstraZeneca (AZ), Bristol-Myers Squibb (BMS), Roche-Ventana, Boehringer Ingelheim, and Ono. C.S. has consulted for Pfizer, Novartis, GlaxoSmithKline (GSK), Merck Sharpe & Dohme (MSD), BMS, Celgene, AZ, Illumina, Genentech, Roche-Ventana, GRAIL, Medicxi, and the Sarah Cannon Research Institute. C.S. is a shareholder of Apogen Biotechnologies, Epic Bioscience, and GRAIL and has stock options in and is co-founder of Achilles Therapeutics. Outside of the submitted work, K.L., S.T., and C.S. have a patent pending on indel burden and CPI response and a patent pending on targeting of frameshift neoantigens for personalized immunotherapy. J.L. reports institutional research support from BMS, MSD, Novartis, Pfizer, Achilles Therapeutics, Roche, Nektar Therapeutics, Covance, Immunocore, Pharmacyclics, and Aveo and consultancy support from Achilles, AZ, Boston Biomedical, BMS, Eisai, EUSA Pharma, GSK, Ipsen, Imugene, Incyte, iOnctura, Kymab, Merck Serono, MSD, Nektar, Novartis, Pierre Fabre, Pfizer, Roche/Genentech, Secarna, and Vitaccess. S.T. has received speaking fees from Astra Zeneca, Novartis, and Ipsen. S.T., K.L., and C.S. have the following patents filed: Clear Cell Renal Cell Carcinoma Biomarkers P113326GB.

Received: June 2, 2019
Revised: September 17, 2019
Accepted: April 1, 2020
Published: May 5, 2020

REFERENCES

AACR Project GENIE Consortium (2017). AACR Project GENIE: powering precision medicine through an international consortium. Cancer Discov. 7, 818–831.

Abbosh, C., Birkbak, N.J., Wilson, G.A., Jamal-Hanjani, M., Constantin, T., Salari, R., Le Quesne, J., Moore, D.A., Veeriah, S., Rosenthal, R., et al.; TRACERx Consortium; PEACE Consortium (2017). Phylogenetic ctDNA analysis depicts early-stage lung cancer evolution. Nature *545*, 446–451.

Andreatta, M., and Nielsen, M. (2016). Gapped sequence alignment using artificial neural networks: application to the MHC class I system. Bioinformatics *32*, 511–517.

Aran, D., Sirota, M., and Butte, A.J. (2015). Systematic pan-cancer analysis of tumour purity. Nat. Commun. *6*, 8971.

Budczies, J., Allgäuer, M., Litchfield, K., Rempel, E., Christopoulos, P., Kazdal, D., Endris, V., Thomas, M., Fröhling, S., Peters, S., et al. (2019). Optimizing panel-based tumor mutational burden (TMB) measurement. Ann. Oncol. *30*, 1496–1506.

Burrell, R.A., and Swanton, C. (2016). Re-evaluating clonal dominance in cancer evolution. Trends Cancer *2*, 263–276.

Carter, S.L., Cibulskis, K., Helman, E., McKenna, A., Shen, H., Zack, T., Laird, P.W., Onofrio, R.C., Winckler, W., Weir, B.A., et al. (2012). Absolute quantification of somatic DNA alterations in human cancer. Nat. Biotechnol. *30*, 413–421.

Cibulskis, K., Lawrence, M.S., Carter, S.L., Sivachenko, A., Jaffe, D., Sougnez, C., Gabriel, S., Meyerson, M., Lander, E.S., and Getz, G. (2013). Sensitive detection of somatic point mutations in impure and heterogeneous cancer samples. Nat. Biotechnol. *31*, 213–219.

Crespi, I. (1988). Pre-Election Polling: Sources of Accuracy and Error (Russell Sage).

David, M. (1988). Handbook of Applied Advanced Geostatistical Ore Reserve Estimation (Elsevier).

Fang, H., Bergmann, E.A., Arora, K., Vacic, V., Zody, M.C., Iossifov, I., O'Rawe, J.A., Wu, Y., Jimenez Barron, L.T., Rosenbaum, J., et al. (2016). Indel variant analysis of short-read sequencing data with Scalpel. Nat. Protoc. *11*, 2529–2548.

Faustino-Rocha, A., Oliveira, P.A., Pinho-Oliveira, J., Teixeira-Guedes, C., Soares-Maia, R., da Costa, R.G., Colaço, B., Pires, M.J., Colaço, J., Ferreira, R., and Ginja, M. (2013). Estimation of rat mammary tumor volume using caliper and ultrasonography measurements. Lab Anim. (NY) *42*, 217–224.

Forde, P.M., Chaft, J.E., and Pardoll, D.M. (2018). Neoadjuvant PD-1 blockade in resectable lung cancer. N. Engl. J. Med. *379*, e14.

Gejman, R.S., Chang, A.Y., Jones, H.F., DiKun, K., Hakimi, A.A., Schietinger, A., and Scheinberg, D.A. (2018). Rejection of immunogenic tumor clones is limited by clonal fraction. eLife *7*, e41090.

Gerstung, M., Beisel, C., Rechsteiner, M., Wild, P., Schraml, P., Moch, H., and Beerenwinkel, N. (2012). Reliable detection of subclonal single-nucleotide variants in tumour cell populations. Nat. Commun. *3*, 811.

Gy, P. (1988). Heterogeneite, Echantillonnage, Homogeneisation (Masson).

Hedley, D.W., Friedlander, M.L., Taylor, I.W., Rugg, C.A., and Musgrove, E.A. (1983). Method for analysis of cellular DNA content of paraffin-embedded pathological material using flow cytometry. J. Histochem. Cytochem. *31*, 1333–1335.

Hellmann, M.D., Ciuleanu, T.E., Pluzanski, A., Lee, J.S., Otterson, G.A., Audigier-Valette, C., Minenza, E., Linardou, H., Burgers, S., Salman, P., et al. (2018). Nivolumab plus ipilimumab in lung cancer with a high tumor mutational burden. N. Engl. J. Med. *378*, 2093–2104.

Jamal-Hanjani, M., Wilson, G.A., McGranahan, N., Birkbak, N.J., Watkins, T.B.K., Veeriah, S., Shafi, S., Johnson, D.H., Mitter, R., Rosenthal, R., et al.; TRACERx Consortium (2017). Tracking the evolution of non-small-cell lung cancer. N. Engl. J. Med. *376*, 2109–2121.

Koboldt, D.C., Chen, K., Wylie, T., Larson, D.E., McLellan, M.D., Mardis, E.R., Weinstock, G.M., Wilson, R.K., and Ding, L. (2009). VarScan: variant detection in massively parallel sequencing of individual and pooled samples. Bioinformatics *25*, 2283–2285.

Lamy, P., Nordentoft, I., Birkenkamp-Demtröder, K., Thomsen, M.B., Villesen, P., Vang, S., Hedegaard, J., Borre, M., Jensen, J.B., Høyer, S., et al. (2016). Paired exome analysis reveals clonal evolution and potential therapeutic targets in urothelial carcinoma. Cancer Res. *76*, 5894–5906.

Li, H., and Durbin, R. (2009). Fast and accurate short read alignment with Burrows-Wheeler transform. Bioinformatics *25*, 1754–1760.

Mariathasan, S., Turley, S.J., Nickles, D., Castiglioni, A., Yuen, K., Wang, Y., Kadel, E.E., III, Koeppen, H., Astarita, J.L., Cubas, R., et al. (2018). TGFβ attenuates tumour response to PD-L1 blockade by contributing to exclusion of T cells. Nature *554*, 544–548.

McGranahan, N., Furness, A.J., Rosenthal, R., Ramskov, S., Lyngaa, R., Saini, S.K., Jamal-Hanjani, M., Wilson, G.A., Birkbak, N.J., Hiley, C.T., et al. (2016). Clonal neoantigens elicit T cell immunoreactivity and sensitivity to immune checkpoint blockade. Science *351*, 1463–1469.

Miao, D., Margolis, C.A., Vokes, N.I., Liu, D., Taylor-Weiner, A., Wankowicz, S.M., Adeegbe, D., Keliher, D., Schilling, B., Tracy, A., et al. (2018). Genomic correlates of response to immune checkpoint blockade in microsatellite-stable solid tumors. Nat. Genet. *50*, 1271–1281.

Nilsen, G., Liestøl, K., Van Loo, P., Moen Vollan, H.K., Eide, M.B., Rueda, O.M., Chin, S.F., Russell, R., Baumbusch, L.O., Caldas, C., et al. (2012). Copynumber: efficient algorithms for single- and multi-track copy number segmentation. BMC Genomics *13*, 591.

Pearson, A., Smyth, E., Babina, I.S., Herrera-Abreu, M.T., Tarazona, N., Peckitt, C., Kilgour, E., Smith, N.R., Geh, C., Rooney, C., et al. (2016). High-level clonal FGFR amplification and response to FGFR inhibition in a translational clinical trial. Cancer Discov. *6*, 838–851.

Quinlan, A.R., and Hall, I.M. (2010). BEDTools: a flexible suite of utilities for comparing genomic features. Bioinformatics *26*, 841–842.

Raynaud, F., Mina, M., Tavernari, D., and Ciriello, G. (2018). Pan-cancer inference of intra-tumor heterogeneity reveals associations with different forms of genomic instability. PLoS Genet. *14*, e1007669.

Rohde, A., Hammerl, J.A., Appel, B., Dieckmann, R., and Al Dahouk, S. (2015). Sampling and homogenization strategies significantly influence the detection of foodborne pathogens in meat. BioMed Res. Int. *2015*, 145437.

Rosenthal, R., McGranahan, N., Herrero, J., Taylor, B.S., and Swanton, C. (2016). DeconstructSigs: delineating mutational processes in single tumors distinguishes DNA repair deficiencies and patterns of carcinoma evolution. Genome Biol. *17*, 31.

Roth, A., Khattra, J., Yap, D., Wan, A., Laks, E., Biele, J., Ha, G., Aparicio, S., Bouchard-Côté, A., and Shah, S.P. (2014). PyClone: statistical inference of clonal population structure in cancer. Nat. Methods *11*, 396–398.

Shukla, S.A., Rooney, M.S., Rajasagi, M., Tiao, G., Dixon, P.M., Lawrence, M.S., Stevens, J., Lane, W.J., Dellagatta, J.L., Steelman, S., et al. (2015). Comprehensive analysis of cancer-associated somatic mutations in class I HLA genes. Nat. Biotechnol. *33*, 1152–1158.

Smith, T., Heger, A., and Sudbery, I. (2017). UMI-tools: modeling sequencing errors in Unique Molecular Identifiers to improve quantification accuracy. Genome Res. *27*, 491–499.

Snyder, A., Makarov, V., Merghoub, T., Yuan, J., Zaretsky, J.M., Desrichard, A., Walsh, L.A., Postow, M.A., Wong, P., Ho, T.S., et al. (2014). Genetic basis for clinical response to CTLA-4 blockade in melanoma. N. Engl. J. Med. *371*, 2189–2199.

Talevich, E., Shain, A.H., Botton, T., and Bastian, B.C. (2016). CNVkit: genome-wide copy number detection and visualization from targeted DNA sequencing. PLoS Comput. Biol. *12*, e1004873.

Thomsen, M.B., Nordentoft, I., Lamy, P., Høyer, S., Vang, S., Hedegaard, J., Borre, M., Jensen, J.B., Ørntoft, T.F., and Dyrskjøt, L. (2016). Spatial and temporal clonal evolution during development of metastatic urothelial carcinoma. Mol. Oncol. *10*, 1450–1460.

Turajlic, S., Xu, H., Litchfield, K., Rowan, A., Horswell, S., Chambers, T., O'Brien, T., Lopez, J.I., Watkins, T.B.K., Nicol, D., et al.; TRACERx Renal Consortium (2018). Deterministic evolutionary trajectories influence primary tumor growth: TRACERx Renal. Cell *173*, 595–610.e11.

Van Loo, P., Nordgard, S.H., Lingjærde, O.C., Russnes, H.G., Rye, I.H., Sun, W., Weigman, V.J., Marynen, P., Zetterberg, A., Naume, B., et al. (2010).

Allele-specific copy number analysis of tumors. Proc. Natl. Acad. Sci. USA *107*, 16910–16915.

Wang, K., Li, M., and Hakonarson, H. (2010). ANNOVAR: functional annotation of genetic variants from high-throughput sequencing data. Nucleic Acids Res. *38*, e164.

Warrick, J.I., Sjodahl, G., Kaag, M., Raman, J.D., Merrill, S., Shuman, L., Chen, G., Walter, V., and Degraff, D.J. (2019). Intratumoral heterogeneity of bladder cancer by molecular subtypes and histologic variants. Eur. Urol. *75*, 18–22.

Wolf, Y., Bartok, O., Patkar, S., Eli, G.B., Cohen, S., Litchfield, K., Levy, R., Jimenez-Sanchez, A., Trabish, S., Lee, J.S., et al. (2019). UVB-induced tumor heterogeneity diminishes immune response in melanoma. Cell *179*, 219–235.e21.

Wong, S.Q., Li, J., Tan, A.Y., Vedururu, R., Pang, J.M., Do, H., Ellul, J., Doig, K., Bell, A., MacArthur, G.A., et al.; CANCER 2015 Cohort (2014). Sequence artefacts in a prospective series of formalin-fixed tumours tested for mutations in hotspot regions by massively parallel sequencing. BMC Med. Genomics *7*, 23.

STAR★METHODS

KEY RESOURCES TABLE

REAGENT or RESOURCE	SOURCE	IDENTIFIER
Antibodies		
Mouse anti-cytokeratin 8/18 antibody	Ventana Medical Systems	cat # 760-4344; RRID:AB_10583331
Goat-anti-Mouse antibodyconjugated with Alexa Fluor 488	Invitrogen	cat # A11001; RRID:AB_2534069
Goat-anti-Mouse antibody conjugated with Alexa Fluor 647	Invitrogen	cat # A-21236; RRID:AB_141725
Chemicals, Peptides, and Recombinant Proteins		
BD FACS Aria	Bectin Dickinson	cat # 656700
CC1 buffer	Ventana Medical Systems	cat # 950-124
antibody diluent buffer	Ventana Medical Systems	cat # 251-018
autoMACS buffer	Miltenyi Biotech	cat # 130-091-221
phosphate buffered saline	Fisher Scientific	cat # 14190
Tween 20	Fisher Scientific	cat # AC233362500
DAPI	Sigma	cat #D9542
Pepsin	Sigma	cat # P7012
Proteinase K	VWR	cat # 0706
Critical Commercial Assays		
cobas cfDNA Sample Preparation Kit	Roche	7247737190
AVENIO ctDNA Enrichment Kit	Roche	8061041001
AVENIO ctDNA Library Prep Kit	Roche	8061050001
HyperCap Target Enrichment Kit, 96 Reactions	Roche	8286345001
SeqCap EZ MedExome Enrichment Kit	Roche	7681330001
NimbleGen SeqCap Hybridization and Wash Kit	Roche	5634253001
HiSeq Rapid SBS Kit v2	Illumina	FC-402-4021
HiSeq SBS Kit V4 250 cycle kit	Illumina	FC-401-4003
xGen Dual Index UMI Adapters	IDT	N/A
SeqCap EZ Prime Choice Probes- Onco	Roche	4000030990- 08247498001
SeqCap EZ Share Choice- Onco	Roche	4000007080- 08332975001
SeqCap EZ Custom Design	Roche	8332975001
SeqCap Adaptor Kit A	Roche	7141530001
HiSeq® 2500 Sequencing System	Illumina	SY-401-2501
cBot System	Illumina	SY-301-2002
20 micron cell strainer	Pluriselect	cat # 43-50020-03
IKA disposable grinding chamber	IKA-Works	cat # MT 40.100
IKA Works Tube Mill Control system	IKA-Works	cat # 0004180001
Deposited Data		
Human reference genome NCBI build 37, GRCh37	Genome Reference Consortium	https://www.ncbi.nlm.nih.gov/projects/genome/assembly/grc/human/
Rep-Seq data for cases RS1-RS12	This paper	European Phenome Genome Archive: EGAS00001004246
Software and Algorithms		
Burrows-Wheeler Aligner (BWA) v0.7.15	Li and Durbin, 2009	http://bio-bwa.sourceforge.net/
Samtools v1.3.1	Li and Durbin, 2009	http://samtools.sourceforge.net/
Picard 1.81		http://broadinstitute.github.io/picard/

(*Continued on next page*)

Continued

REAGENT or RESOURCE	SOURCE	IDENTIFIER
Mutect v1.1.7	Cibulskis et al., 2013	http://software.broadinstitute.org/cancer/cga/mutect
VarScan v2.4.1	Koboldt et al., 2009	http://varscan.sourceforge.net/
Scalpel v0.5.3	Fang et al., 2016	https://github.com/hanfang/scalpel-protocol
Annovar	Wang et al., 2010	http://annovar.openbioinformatics.org/en/latest/
CNVkit v0.7.3	Talevich et al., 2016	https://github.com/etal/cnvkit
R package 'Copynumber'	Nilsen et al., 2012	http://bioconductor.org/packages/release/bioc/html/copynumber.html
ABSOLUTE v1.0.6	Carter et al., 2012	http://software.broadinstitute.org/cancer/cga/absolute
bedtools package	Quinlan and Hall, 2010	https://bedtools.readthedocs.io/en/latest/
AlleleCounter	N/A	https://github.com/cancerit/alleleCount
ASCAT	Van Loo et al., 2010	https://github.com/Crick-CancerGenomics/ascat

LEAD CONTACT AND MATERIALS AVAILABILITY

Further information and requests for resources and reagents should be directed to and will be fulfilled by the Lead Contact, Samra Turajlic (samra.turajlic@crick.ac.uk). This study did not generate new unique reagents.

EXPERIMENTAL MODEL AND SUBJECT DETAILS

Clinical studies

Cases RS1, RS3 and RS4 were diagnosed with renal cell carcinoma, and were consented for research under the TRACERx Renal study (National Health Service Research Ethics Committee approval 11/LO/1996), as previously described[5]. Autopsy samples from RS1 and RS2 were obtained through the PEACE Study (NIHR 18422), where samples are harvested within ~48 hours from death (see secondary author list for the full list of PEACE consortium investigators). Residual surgical material for cases RS5, RS6, RS7, RS8, RS9, RS10, RS11 and RS12 were was obtained from commercial providers of research specimens (GLAS Consultants, Winston-Salem, NC. (IRB#: 120160685) and The MT Group, Van Nuys, CA (MTG-015)) from U.S. hospitals, under IRB approval. Sex/age of each case is as follows: RS1 M/54, RS2 M/41, RS3 M/75, RS4 F/75, RS5 F/55, RS6 F/81, RS7 F/90, RS8 M/65, RS9 M/83, RS10 F/68, RS11 F/75, RS12 (n.a.).

METHOD DETAILS

Clinical audit of current molecular profiling practices

Institutional review board approval was obtained for a service evaluation to quantify the tumor volume routinely profiled as a diagnostic standard of care in resected colorectal, melanoma and sarcoma tumors (SE725), where surgery and molecular profiling were both undertaken at the Royal Marsden NHS Foundation Trust was reviewed. Cases were included if there were > 2 macroscopic tumor dimensions recorded on the histopathology report and if information was available on the number and thickness of slides used for molecular profiling. The audit data is shown in Table S4.

Regional biopsy and cocktail sample preparation

Multi and single region biopsy sampling of surgically resected tumor tissue was conducted using the same method as previously described (Turajlic et al., 2018). Cocktail samples (as displayed in Figure 1) were created for each tumor, by pooling extracted DNA taken from all single-regions taken for each tumor, in equimolar ratios. A median of 9 single—region samples were pooled per cocktail. For the autopsy samples from RS1 and RS2, $3mm^3$ sections were dissected from snap frozen tumor core biopsies (6mm diameter) and tissue disrupted using the Tissue Raptor. They were then processed through a QIAGEN QIAshredder and DNA was purified using the QIAGEN All Prep DNA/RNA Mini kit according to manufacturer's instructions. Germline DNA was extracted from whole blood or a buffy coat.

Grossing and homogenization of residual tumor tissue

Following diagnostic histologic sampling and removal of fresh biopsies, three distinct clinical surgical waste tissues from a kidney radical nephrectomy (RS1) containing: 1) a primary tumor, 2) para-aortic lymph node cluster, and 3) renal hilar nodes were fixed in

10% neutral buffered formalin for 24 h to mimic the standard clinical workflow. After fixation, samples were exchanged into phosphate-buffered saline (PBS, 14190, Fisher Scientific, USA) for 24 h, then stored in ethanol for until dissected. Tumor tissue was identified by a pathologist through macroscopic evaluation and physical palpation, and all identifiable tumor was dissected away from the surrounding tissue. An area of normal tissue (at least 5 cm from the tumor) was also dissected by a pathologist and retained. Lymph nodes detected during gross examination of the RS1 specimen included hilar and peri-renal nodes were also dissected as an independent tissue samples. All dissected tissue was weighed prior to homogenization.

Residual primary tumor tissue was split into two-625 g portions; each portion was combined with 600 mL autoMACS Running Buffer (Miltenyi Biotec Inc., 130-091-221) and homogenized in a liquidizer (Cookworks, BL9292E-GS) for 3 min at the highest setting. The primary tumor homogenates (2.5 l total) were manually combined and mixed in a plastic container, divided back and re-liquidized for additional homogenization and mixing, and pooled together into a large plastic container. Segregated tissues of renal hilar lymph nodes, peri-renal node, normal kidney tissue, and para-aortic lymph nodes were each homogenized independently in autoMACS Running Buffer (1:1, mass: volume) with an IKA Tube Mill (IKA Works Inc. Wilmington North Carolina, 0004180001) for 2 min at 15,000 rpm using single-use blending containers. When tissue mass exceeded the capacity of an individual blender container, homogenates for the same sample were pooled by mixing as described above. Samples of each tissue homogenate were stored in methanol (1:1, v:v) at 4°C. Case RS2 was lymph-node material from a patient with primary melanoma, and cases RS3 and RS4 were primary renal tumors, and all were processed through the same homogenization protocol as RS1. For RS2 primary melanoma tissue, the FFPE blocks were trimmed by razor-blade to remove excess paraffin wax that did not contain any tissue. Remaining wax embedded tissue was removed from FFPE plastic cassette and minced into approximately 1mm cubed pieces using razor blade. Tissue pieces were deparaffinised by 5 sequential 1.5 hour 52 degrees' Celsius xylene washes until all but trace wax was removed and only tissue remained. Xylene was removed from the sample using a room temperature 10 minute acetone wash followed by three sequential 20 minute 100% ethanol washes. Ethanol was removed, and the sample hydrated for blending, in two 10 minute sequential washes of 1x PBS.

For cases RS5 to RS12, each specimen had been subjected to standard sampling for diagnosis and staging purposes. These cases were considered surgical waste and slated for incineration, thus were stored in formalin for four to six weeks. Upon arrival, tissue was transferred to PBS for 12-24h. Tumor tissue was identified by a pathologist through macroscopic evaluation and physical palpation, and all identifiable tumor was dissected away from the surrounding tissue. An area of normal tissue (at least 5 cm away from the tumor) was also dissected by a pathologist and retained. All dissected tissue was weighed prior to homogenization. Dissected tumor and normal tissue were homogenized separately in single-use blender containers (IKA Works Inc. Wilmington North Carolina, 0004180001), or single use consumer grade blenders (Hamilton Beach, 51102, Glen Allen, VA) in autoMACS buffer (1:1, m:v) for 2 min at 15,000 rpm or at the highest setting. Resulting homogenates were stored at 4°C until further processed.

Genomic DNA purification from tissue and cfDNA

An aliquot of each tissue homogenate (1200 μl) was collected by centrifugation at 5000 *rcf.* for 2 min, rinsed with TE buffer pH 8.0 (VWR, AAJ62745-EQE) twice, and incubated in 5 mL protease digestion buffer [9.75 mL TE buffer pH 8.0, 60 mg Proteinase K (VWR, 0706), and 0.25 mL 20% SDS in aqueous solution (Amresco, 0837)] at 56°C for 2-16 h. Digested tissue (100 μl) was used for genomic DNA purification by High Pure PCR Purification Kit (Roche Applied Sciences, Mannheim Germany, 11 732 668 001) according to manufacturer's protocol. Purified genomic DNA was quantified using a NanoDrop 8000 (Thermo Fisher Scientific) and stored at −20°C. cfDNA was isolated from plasma using cobas cfDNA Sample Preparation kit (Roche, 07247737190).

Target-enriched NGS Library construction and sequencing

Illumina compatible indexed NGS libraries were constructed from genomic DNA from tissue using the SeqCap EZ HyperCap Workflow User's Guide, v1.0 (Roche Sequencing Solutions) with notable parameters specified below. Briefly, 1 μg of purified genomic DNA was enzymatically fragmented for 33-40 min at 37°C and prepared for adaptor ligation using the KAPA HyperPlus library prep kit according to manufacturer's instructions (Roche Sequencing Solutions, KK8514). SeqCap sequencing adaptor final reaction concentration was 2 μM, and adaptor ligation reaction time was extended to 14-18 h, at 16°C. No pre-capture PCR was used following ligation reaction purification. SeqCap EZ library probe baits for either MedExome (07681330001), Onco_EZ (08333076001), or a custom RS1 specific (see data analysis section below for design criteria) target-enrichment panel (Roche Sequencing Solutions) and 2 nM blocking oligos (Roche Sequencing Solutions), were incubated for 18-22 h at 47°C following manufacturer instructions. Post-capture PCR was performed using KAPA HiFi HotStart ReadyMix and LM-PCR oligos for 14 cycles. Post-capture purified library concentrations were determined by Qubit (ThermoFisher) and fragment size distribution analyzed by Bioanalyzer 2100 (Agilent). Amplified enriched libraries were each diluted to 2nM and stored at −20°C prior to pooling for sequencing. Pooled libraries were sequenced using MiSeq and HiSeq instruments (Illumina) according to manufacturer's recommendations for paired-end sequencing using (Illumina) runs with 101 base paired-end reads. cfDNA sequencing libraries were constructed using the AVENIO ctDNA Targeted Kit (Roche, 08061076001) by following the AVENIO ctDNA Analysis Kits Reagent Workflow User Guide v1.0.0. Amplified, adaptor-ligated samples were concentrated together with the Hybridization Supplement using a Vacufuge plus instrument (Eppendorf). Each sample was resuspended in the appropriate Enhancing Oligo, the custom RS1-specific panel, and Hybridization master mix. Enrichment, hybridization cleanup and amplification were performed according to manufacturer instructions. Samples (equal mass) were pooled, and sequenced using Hiseq (Illumina), according to instructions, with 151 base paired-end reads. Multi-region, cocktail and single regions samples, from 79 renal cell carcinomas as displayed in Figure 1, underwent renal driver

Panel_v6 library preparation and sequencing, using methods as previously described (Turajlic et al., 2018). Multi-region whole exome library preparation and sequencing for RS1 was conducted by external laboratory (Eurofins Scientific), using Agilent SureSelect Human All Exon v5 kits. Multi-region whole exome library preparation for RS2 was conducted at the UCL Pathogen Genomics Unit, using Agilent SureSelect Human All Exon v5 kits, and sequenced by external laboratory (GENWIZ). Sequencing coverage metrics, and library kits, for all samples profiled is provided in Table S5.

Flow sorting method to increase tumor purity

A representative sample from formalin fixed residual tumor tissue from RS12 was generated by homogenization in an IKA blender in autoMACS buffer (1:1 mass to volume). Aliquots of the homogenate (1 g) were further dissociated to individual nuclei by adapting a previously described method (Hedley et al., 1983). Briefly, tissue was collected by centrifugation, resuspended in CC1 (Ventana Medical Systems, Tucson, AZ) buffer (5:1 mass to volume), and heated at 80°C for 30 min. Tissue was washed once with PBS, and resuspended in PBS containing 1 mg/ml proteinase K (1:1 mass to volume) (VWR USA) and incubated at 50°C for 10 min. The sample was exchanged into 5 mg/ml pepsin in 150 mM NaCl, pH 1.5 (Sigma, USA) and incubated 30 min at 37°C. The sample was adjusted to pH 8 with 5 M NaOH, and exchanged into PBS, 0.5% BSA and 0.5% Tween 20 (Fisher Scientific, USA (AC233362500) prior to filtration through a 20-μm filter (Pluriselect, San Diego, CA) to collect nuclei.

Nuclei were then collected by centrifugation at 400 x g and exchanged into antibody diluent for 30 min at 20°C. Samples were exchanged into mouse anti-cytokeratin 8/18 primary antibody (Ventana Medical Systems, Tucson, AZ) for 1 hour at 4°C, washed three times in 0.5 mL PBS, 0.1% BSA and 0.1% Tween 20, and incubated for 30 min at 4°C in goat-anti-mouse antibodies conjugated to Alexa Fluor 488 or Alexa Fluor 647 (2 μg/ml) (Invitrogen, San Diego, CA) and DAPI (3 μM) (Sigma, USA). Stained samples were washed and filtered prior to analysis and sorting using a BD FACS Aria (656700, Bectin Dickinson) equipped with a 355 nm, 60 mW laser and 450/50 nm filter for DAPI; 488 nm, 60 mW laser and 530/30 nm filter for AF 488; and 633 nm, 100 mW laser and 670/30 nm filter for AF 647. No compensation was used. DAPI was used for doublet discrimination. RS11 tumor nuclei were enriched by FACS after gating to include cytokeratin positive (CK+), high side-scatter (SSC) nuclei and exclude cytokeratin negative (CK-), low SSC nuclei. The flow cytometry gating strategy is shown in (Figure S5).

QUANTIFICATION AND STATISTICAL ANALYSIS

Tumor volume sampling analysis

For the the clinical audit data, all samples had data on width (W) and length (L) dimensions available, and tumor volume (T_V) was estimated using the following formula:

$$T\_V = (W^2 \times L)/2$$

(taken from the literature as the most accurate tumor volume measurement approach (Faustino-Rocha et al., 2013)).

Biopsy volume (B_V) was calculated based on the 2D surface area analysis of 8 typical slides, with each slide scanned using the Aperio AT2 whole slide scanner at 40x. Each image was annotated by hand, following the perimeter of the tissue, and the surface area calculated via using the Aperio ImageScope software. The average surface area was 3.37cm^2 and this value was multiplied by slide thickness (10 μm), and the total number of slides used, to obtain B_V estimates per tumor. We note that in cases where multiple slides were used for molecular profiling, (up to 5 were used), each slide was taken from the same block (i.e., all from one fixed spatial location). The proportion of total tumor volume sampled in each case is then simply calculated as B_V / T_V. For the cancer genome atlas (TCGA) dataset analysis, we extracted summary clinical annotation files for each solid tumor cohort from the Broad Institute TCGA GDAC Firehose repository. Tumor dimension data was available for n = 1667 samples, across 6 tumor types: ACC, KICH, KIRC, KIRP, PAAD and THCA. Tumor volume (T_V) was calculated as per above using the formula: $T\_V = (W^2 \times L) / 2$. In cases where only one dimension was given (i.e., the maximal dimension) this was assumed to be the tumor length, and the tumor width was estimated using a L:W ratio of 1:0.8, with the 0.8 standard value estimated as the median ratio value observed across all cases with available length and width data. Biopsy sample volumes were calculated from exact length (L), width (W) and depth (D) dimensions, as given in the clinical annotation files, with biopsy shape assumed to be cuboid and biopsy volume (B_V) calculated as $B\_V = L \times W \times D$. Where biopsy dimensions were missing in the clinical annotation files, a standard biopsy volume (B_V) of 0.48cm^3 was assumed, based on the median value from all other bases where data was available. The proportion of total tumor volume sampled in each case is then simply calculated as B_V / T_V. In Figure 1A, significance was assessed with a Wilcoxon rank-sum test. In Figure S1 the intratumor heterogeneity scores, for cases overlapping with the proportion of tumor sampled dataset, were taken from (Raynaud et al., 2018) (number of clones score). Purity estimates, again for TCGA cases overlapping with the proportion of tumor volume sampled analysis, were taken from (Aran et al., 2015) (consensus purity estimates).

Processing of sequencing data

Paired-end reads in FastQ format sequenced by MiSeq and Hiseq were aligned to the reference human genome (build hg19), using the Burrows-Wheeler Aligner (BWA) v0.7.15. with seed recurrences (-c flag) set to 10000 (Li and Durbin, 2009). Intermediate processing of Sam files was performed using Samtools v1.3.1, deduplication was performed using Picard 1.81 (http://broadinstitute.github.

io/picard/) and local indel realignment with GATK v3.6. For whole exome and renal driver Panel_v6 sequencing datasets, single Nucleotide Variant (SNV) calling was performed using Mutect v1.1.7 and small scale insetion/deletions (INDELs) were called running VarScan v2.4.1 in somatic mode with a minimum variant frequency (–min-var-freq) of 0.005, a tumor purity estimate (–tumor-purity) of 0.75 and then validated using Scalpel v0.5.3 (scalpel-discovery in - -somatic mode) (intersection between two callers taken) (Cibulskis et al., 2013, Fang et al., 2016, Koboldt et al., 2009). SNVs called by Mutect were further filtered using the following criteria: i) variant allele frequency (VAF) $\leq$ 1% in the corresponding germline sample, ii) variants that falling into mitochondrial chromosome, haplotype chromosome, HLA genes or any intergenic region were not considered, iii) presence of both forward and reverse strand reads supporting the variant. For custom RS1 panel sequencing data, sequencing was conducted at high depth using unique molecular barcode (UMI) indexes, and UMI-tools (Smith et al., 2017) was used to group PCR duplicates and de-duplicate reads to yield one read per group. SNVs were then called using deepSNV (Gerstung et al., 2012), as Mutect is known to not be calibrated for higher sequencing depth levels. Varscan and Scalpel were used to call RS1 custom panel INDELs as described above. All variants were annotated using Annovar (Wang et al., 2010). To estimate somatic copy number alterations, CNVkit v0.7.3 was performed with default parameter on paired tumor-normal sequencing data (Talevich et al., 2016). Outliers of the derived logR calls from CNVkit were detected and modified using Median Absolute Deviation Winsorization before case-specific joint segmentation to identify genomic segments of constant logR (Nilsen et al., 2012). Tumor sample purity, ploidy and absolute copy number per segment were estimated using ABSOLUTE v1.0.6 (Carter et al., 2012). Neoantigen predictions were derived by first determining the 4-digit HLA type for each patient, along with mutations in class I HLA genes, using POLYSOLVER (Shukla et al., 2015). Next, all possible 9, 10 and 11-mer mutant peptides were computed, based on the detected somatic non-synonymous SNV and INDEL mutations in each sample. Binding affinities of mutant and corresponding wild-type peptides, relevant to the corresponding POLYSOLVER-inferred HLA alleles, were predicted using NetMHCpan (v3.0) and NetMHC (v4.0) (Andreatta and Nielsen, 2016). Neoantigen binders were defined as $IC_{50} < 50$ nM or rank < 2.0. Signature analysis was conducted on all non-synonymous mutations using package deconstructSigs (Rosenthal et al., 2016). We additionally checked for evidence of formalin induced artifact variants in the Rep-Seq data, given the protocol involves formalin exposed material. Formalin fixed paraffin embedded (FFPE) samples can contain artifacts, typically arising due to hydrolytic deamination of cytosine to form uracil, or thymine if the cytosine is methylated. Such artifacts are normally visible as an excess of C > T/G > A mutations at lower variant allele frequency (Wong et al., 2014). Analysis of this in the whole exome sequencing data from Rep-Seq cases showed no evidence of excess low frequency formalin induced artifact, with the proportion of low frequency (below 5% VAF) C > T mutations being 34.0%, closely comparable to the average across all base changes (33.3%) (Figure S5).

Analysis of pooled cocktail sequencing data

The final set of cocktail samples included 79 tumors with matched processed reference datasets from multi-region sequencing. The number of biopsies per cocktail sample ranged from 2 to 75 with a median number of 8 biopsies per tumor and a total number of 1,184 individual biopsies. As a reference dataset of true variants, we used previously published multi-region sequencing variant calls from the same cases, which represented the sum of all variants detected in each tumor (Turajlic et al., 2018). In our analysis we compared the overall performance of single-region and cocktail sequencing, in detecting somatic mutations from the known truth set. The single region sample was selected as one random single-region biopsy per tumor, from the overall multi-region dataset. We first evaluated the performance of the cocktail sequencing approach compared to multi-region and single region sequencing, by comparing the number of somatic variants detected per tumor with each approach. To reflect the average performance of single region biopsies, we calculated the mean number of variants detected through single-region sequencing per tumor. We next determined the detection rates of true variants in the cocktail and the single-region samples using the multi-region sequencing data as a reference. Significance was assessed with a paired Wilcoxon Test. Finally, in order to establish the accuracy of the cocktail sequencing approach, we next determined the correlation between the variant allele frequencies (VAF) of all somatic mutations detected through multi-region sequencing and the VAFs from the cocktail samples as well as a randomly selected single-region biopsy per tumor. The multi-region VAFs were calculated as the mean VAFs across all regions included in the cocktails. The correlations were calculated with a Spearman's rank-order correlation test.

Analysis of in-silico pooled cocktail sequencing data

For the analysis presented in Figures 1E and 1F, we made use of two additional multi-region sequencing datasets: i) the TRACERx100 non-small cell lung cancer dataset (Jamal-Hanjani et al., 2017) and ii) a cohort of urothelial carcinomas (Lamy et al., 2016, Thomsen et al., 2016). Each multi-region sample had undergone whole exome sequencing, as described previously described (Lamy et al., 2016, Thomsen et al., 2016, Jamal-Hanjani et al., 2017). Sequencing reads were reverted back to fastq format using bam2fastq, and alignment/variant calling was conducted as described above. The *in-silico* cocktail samples were created for each case by down-sampling the reads in each biopsy sample using picard-tools ''DownsampleSam,'' and then remerging the down-sampled BAM files to make a merged *in-silico* cocktail sample. The down-sampling proportion was selected to ensure the merged *in-silico* cocktail sample had equivalent coverage to a single biopsy samples for that tumor (e.g., if a tumor had five different biopsy samples sequenced, a proportion of 0.2 of each BAM was taken to create a merged file of equivalent depth to a single biopsy). For each dataset, TMB was measured as the number of missense variants per tumor, with a high TMB threshold of 200 missense mutations used, which prior analysis has shown is equivalent to the 10 mutations/Mb threshold (synonymous and non-synonymous) derived from

higher coverage panel datasets (Budczies et al., 2019). The TMB values were calculated using three different methods: A) Single biopsy-TMB, based on the number of mutations in each individual biopsy sample. B) clonal-TMB, based on the full multi-region data for each tumor, with mutations being judged as clonal by simple ubiquity across all tumor regions. C) Cocktail-TMB, based on the number of predicted clonal mutations within the *in-silico* cocktail, with clonality determined by clustering variant allele frequency values using R function daisy, with the distance matrix computed using Gower's formula, and the number of clusters set to two (such that mutations were grouped into either clonal/subclonal groups).

Custom panel design

To conduct in-depth validation of the representative sequencing method high coverage profiling was conducted in case RS1, using a custom panel. The panel design was based on whole exome sequencing results from: i) 7 biopsies taken from the RS1 primary tumor (before homogenization) and ii) an aliquot of the RS1 homogenized solution. SNV and INDEL mutations were called across the 8 samples as described above, and a total of 76 non-synonymous mutations were detected (Table S6). These 76 mutations were successfully captured in a targeted custom panel, and sequenced to high depth (median > 10,000x) in the 64 primary biopsies, 11 biopsies taken from 2 lymph node metastases, 4 biological primary Rep-Seq replicates, 6 circulating tumor (ct) DNA samples collected at different time points, and 3 homogenized lymph node Rep-Seq samples. As an additional validation, all 76 RS1 variants were also validated using Ion Torrent sequencing, as orthogonal confirmation.

Jaccard reproducibility analysis

The reproducibility of variant discovery between RS1 tumor biopsies, Rep-Seq biological replicates and ctDNA samples was assessed using the Jaccard similarity coefficient. Each pairwise combination between samples (within each group) was considered, e.g., Biopsy1 (A) versus Biopsy2 (B), Biopsy1 (A) versus Biopsy3 (B), etc. Jaccard similarity coefficient was calculated using the standard formula (J):

$$J = M_{11}/(M_{01} + M_{10} + M_{11})$$

where M_{11} represents the total number of variants present in both samples A and B, M_{10} represents the total number of variants present in A but not B and M_{01} represents the total number of variants present in B but not A.

Clustering and phylogenetic analysis

Clustering analysis was performed on cases RS1 (custom panel data) and RS2 (whole exome data) using PyClone Dirichlet process clustering (Roth et al., 2014). For each mutation, the observed alternative allele count, reference count and total local tumor copy number was used as input, together with the purity for each sample. PyClone was run with 10,000 iterations and a burn-in of 1000, and default parameters, with–var_prior total_copy_number. For RS1, two separate PyClone runs were conducted, the first for the primary multi-region biopsies dataset. Of the total n = 64 primary biopsies sequenced, n = 52 passed quality control for clustering analysis, with n = 12 biopsies excluded due to lower purity (measured based on purity being too low to call the known clonal 3p copy number loss event correctly). The second RS1 PyClone clustering run was conducted just for Rep-Seq homogenate sample alone (n = 1), using the same parameters. Similarly, three separate PyClone runs were conducted for case RS2, for single biopsy LN sample (alone), Rep-Seq LN sample (alone) and then all biopy samples (from LN and eight other sites of metastases).

Illusion of clonality simulation

To assess the risk of illusion of clonality, a biopsy sampling approach was simulated, for 1 up to 20 biopsies taken, using the RS1 datatset. For each biopsy number (n = 1-20), a random sample of biopsies of size n was drawn from the total set of 64 primary biopsies profiled for RS1. Within the random sampled set, the number of mutations which appeared to be clonal (based on being ubiquitously present in all biopsies in the sampled set) was calculated. This list was then compared to the known list of truly clonal mutations (from the full 64 set), and percentage of variants which were incorrectly classified as clonal was recorded. This process was repeated for 100 iterations for each n, to give a distribution, from which mean and standard deviation values were calculated.

Analysis of purity enriched data

For RS12, whole exome sequencing case conducted using the standard Rep-Seq protocol, and then repeated with the additional step of flow sorted purity enrichment. Variant calling was completed, and purity estimates calculated in both samples in the same way, as detailed above. The number of variants discovered in each sample, and then those in common across samples were calculated and plotted in Figure 5.

Statistical methods

Statistical package R v3.3.2 or higher was used for all analysis. All statistical tests were two-sided. The tests used for each analysis are listed above in the relevant methods section.

DATA AND CODE AVAILABILITY

Sequencing data that supports this study has been deposited at the European Genome-phenome Archive (EGA), which is hosted by the European Bioinformatics Institute (EBI); under accession number EGAS00001004246. The TRACERx lung exome sequence data used during the study is available through the Cancer Research UK & University College London Cancer Trials Centre (ctc.tracerx@ucl.ac.uk) for non-commercial research purposes, and access will be granted upon review of a project proposal that will be evaluated by a TRACERx data access committee and entering into an appropriate data access agreement subject to any applicable ethical approvals.